



## School of Chemistry

The growth of single-crystal diamond on iridium-coated sapphire using pulsed DC-CVD systems

Cheuk Hei LUI

**This thesis is submitted in partial fulfilment of the requirements for the Honours Degree of BSc at the University of Bristol.**

April 2024

Supervisor: Professor Neil A. Fox  
2<sup>nd</sup> assessor: Professor Paul W. May

## Sections

1. Statement of factors which limited project progress
2. Abstract
3. Acknowledgements
4. Introduction
  - 4.1. Diamond as a Useful Material
  - 4.2. Structure of Diamond
  - 4.3. Synthetic Diamond
    - 4.3.1. High-Pressure High-Temperature Method
    - 4.3.2. Chemical Vapour Deposition
      - 4.3.2.1. General Chemical Mechanism
      - 4.3.2.2. Gas Activation
      - 4.3.2.3. Choice of Substrate
  - 4.4. Spectroscopic Methods
    - 4.4.1. Raman Spectroscopy
    - 4.4.2. Scanning Tunneling Microscopy/Atomic Force Spectroscopy
    - 4.4.3. X-Ray Diffraction
    - 4.4.4. Scanning Electron Microscopy
    - 4.4.5. Optical Emission Spectroscopy
  - 4.5. Project Details
5. Experimental
  - 5.1. CVD Diamond on Molybdenum
  - 5.2. CVD Diamond on Iridium/sapphire
  - 5.3. Optical Emission Spectroscopy
  - 5.4. Raman Spectroscopy
6. Results & Discussion
  - 6.1. Diamond Grown on Molybdenum and Ir/sapphire
  - 6.2. Graphitic Film on Molybdenum Disc
7. Conclusion
8. Reference
9. Appendix
  - 9.1. Raman Spectroscopy of the Mo Substrate from the 2<sup>nd</sup> CVD Reaction
  - 9.2. Raman Spectroscopy of the Ir/sapphire Substrate on Mo disc from the 2<sup>nd</sup> CVD Reaction
  - 9.3. Optical Emission Spectroscopy of the 2<sup>nd</sup> CVD Reaction
  - 9.4. Lab Clearance Form

## 1. Statement of factors which limited project progress

The project was delayed by several factors. The project's original plan was to carry out chemical vapour deposition (CVD) using The 'Minion', a CVD reactor in the Diamond Lab. However, the reactor was not ready for experiments immediately. Weeks were spent cleaning the reactor parts and waiting for the components to be delivered or cleaned by the Mechanical Workshop. On top of that, staff getting illnesses resulted in delayed start of the cleaning process. The Balzers reactor experiment was disrupted by the fire evacuation in the School of Physics.

A few instrument failures (other than the Minion reactor) could have potentially affected the project's progress, including the failure of the microwave reactor (for further growing diamonds after the DC-CVD reaction) and the water cooling system of the laser machine (for cutting the iridium-sapphire crystals into chips).

The issues mentioned above delayed the first experiment by nearly two months until late February, eventually limiting the number of experiments that could be carried out and reducing the variety of possible spectroscopy to be carried out (with the expected waiting time for the data to be returned being later than the thesis submission date).

## 2. Abstract

Diamonds have long been one of the most important materials due to their superior properties. These properties open a wide variety of potential applications, from mechanical tools to nanotechnologies, but at the same time, they increase the demand for synthetic diamonds. One of the synthetic methods is known as chemical vapour deposition (CVD), which involves the deposition of carbon from an activated carbon-containing gas to a substrate. Studies show that iridium-coated sapphire has the ideal lattice structure for heteroepitaxially growing single-crystal diamonds.

In this study, a pulsed-DC CVD system was used to study the effects of different parameters on the growth of diamonds, including the choice of substrate, methane concentration and the electrodes' power. The product samples were studied using Raman spectroscopy. In the spectra, peaks appeared at  $1333.22\text{ cm}^{-1}$  and  $1333.61\text{ cm}^{-1}$ , which were similar to the literature value for the Raman shift of diamonds ( $1332\text{ cm}^{-1}$ ). The results suggested that diamonds were successfully nucleated and grown on an Ir/sapphire substrate. A lower temperature and methane concentration could have promoted the formation of crystalline diamond structure over the graphitic structure. However, more spectroscopic measurements are required to understand the structural details of the product crystals, including the crystal orientations and the surface topography. Further research is also needed to thoroughly investigate the effects of different reaction conditions on the purity and the rate of diamond crystal growth.

On the other hand, an iridescent layer of film was formed onto the molybdenum disc that supported the Ir/sapphire in the reactor. The layer was composed of majorly graphitic structures. This confirms the literature on Ir/sapphire being an ideal substrate for CVD diamonds. Further studies are required to investigate the possibility of synthesising multiple carbon compositions simultaneously.

### **3. Acknowledgements**

Firstly, I would like to thank my supervisor, Professor Neil Fox, for supporting and guiding the completion of the project despite all the disruptions that occurred in the past few months.

I would also like to express my gratitude to Dr James Smith for guiding and supporting my project throughout this short journey in the Diamond Lab, including my very first time using a Raman spectroscopy system. Although the 'Minion' reactor was not used in this project in the end, it was a very precious and enjoyable experience to be able to help clean the reactor.

I would like to thank Ms Catherine Monk for cutting the Ir/sapphire chips and Mr Ian Bickerton for using the software to control the Balzers CVD reactor.

I would like to thank Dr Remiz Zulkharnay, Mr Liam Cullingford, and everyone at the Diamond Group for creating an enjoyable working atmosphere.

With all the pressure of studying and life, I would like to thank my family for encouraging me in my daily life. I would also like to thank my brothers and sisters in the Living Water Fellowship for sharing my worries, encouraging me, keeping me with a work-life balance, and guiding me back to Christ.

Last but most importantly, I am grateful for God's guidance, blessings and love. Without You, I can do nothing.

'Do not be anxious about anything, but in every situation, by prayer and petition, with thanksgiving, present your requests to God. And the peace of God, which transcends all understanding, will guard your hearts and your minds in Christ Jesus.'

Philippians 4:6-7, NIV

## 4. Introduction

Since its discovery thousands of years ago, diamonds have been one of the most valuable materials. Its shiny appearance attracted people to use it in jewellery. In recent decades, people have gained an understanding of this special material and found a number of unique properties which can be used in many different industries. <sup>1</sup>With an increasing demand for various applications, humans have been searching for an optimal method for synthesising diamonds.

### 4.1. Diamond as a Useful Material

Diamond exhibits a range of superior properties that other materials can hardly compete with. For example, it is the hardest and stiffest material. At room temperature, it has the highest thermal conductivity ( $2 \times 10^3 \text{ Wm}^{-1} \text{ K}^{-1}$ ), which makes it a very good candidate for heat bank or heat dissipation. <sup>2,3</sup> It is an excellent electrical insulator (ca.  $10^{16} \Omega \text{ cm}$ ). <sup>2</sup> When the crystal is doped with elements like boron or phosphorus, it creates extra electrons or holes within the crystal structure, making it a *p*-type or *n*-type semi- or even super-conductor. <sup>4,5</sup> It also has an ultra-wide band gap (5.48 eV at 300 K), which allows the electronic components to remain stable under harsh electronic environments. <sup>5-7</sup> Moreover, it is chemically inert and biocompatible. <sup>8</sup>

By combining these properties, diamonds have a wide range of applications. For example, diamonds are applied to electric and electronic components. Chemically inert diamonds are an excellent candidate for protecting batteries from corrosion. <sup>9</sup> On the other hand, diamonds are applied in integrated circuits. At such microscopic levels of size, efficient heat dissipation becomes important. Manufacturers, hence, make use of the high thermal conductivity of diamonds and create silicon-diamond multilayer substrates to overcome the problem. <sup>3</sup> Being the hardest and stiffest, diamonds are also highly used in mechanical tools. <sup>10</sup> Scratch-free windows become possible as well. <sup>11</sup> Besides, diamonds are also widely used in biotechnologies and nanotechnologies like biosensors because they are chemically inert and biocompatible. <sup>8, 12, 13</sup>

### 4.2. Structure of Diamond

Diamond is one of the carbon allotropes, with carbon atoms tetrahedrally bonded together in a face-centred cubic close-packed crystal structure (*Fig. 1*). <sup>14</sup> With a dense network of carbon-carbon single bonds, diamond is a thermodynamically stable carbon allotrope along with graphite, especially when under high-pressure conditions. <sup>2</sup>

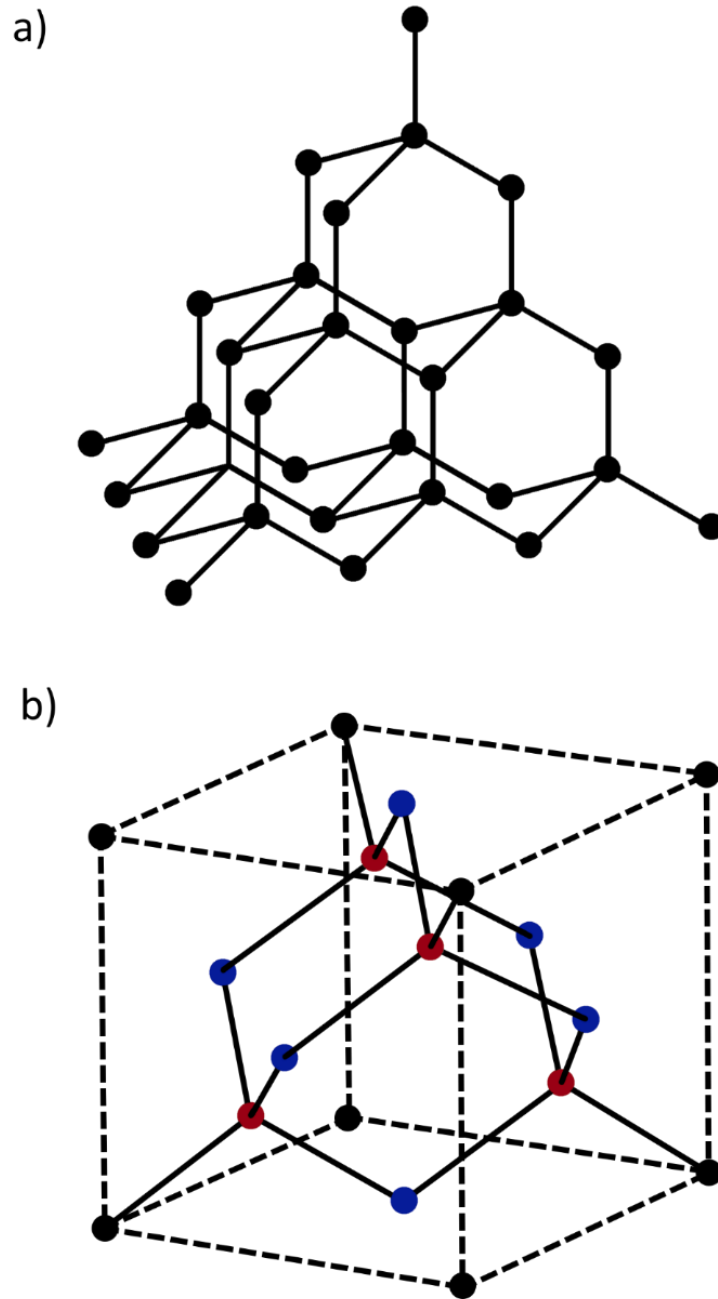


Figure 1: (a) Structure of diamond. (b) Lattice of diamond. The circle represents the carbon atoms, with black being on the vertices of the lattice, blue at the centre of the faces, and red inside the lattice. Figure modified from the original in [15].

For crystalline structures like diamonds, the surface of the crystal can be in different orientations. The most discussed diamond planes are the  $\langle 100 \rangle$  and  $\langle 111 \rangle$  surface planes, as they are commonly formed in lab-synthesised diamonds (Fig. 2).<sup>17</sup> The orientations of the two planes are diagonal to each other. With different orientations, the atomic arrangements and the activities of the two surfaces become different from each other. For the  $\langle 100 \rangle$  surface plane, the atoms are arranged like a square array. For the  $\langle 111 \rangle$  plane, this becomes triangular-like (Fig. 3).<sup>18</sup> The difference in atomic arrangements affects surface activities, hence their properties and potential applications (Fig. 4).<sup>17</sup>

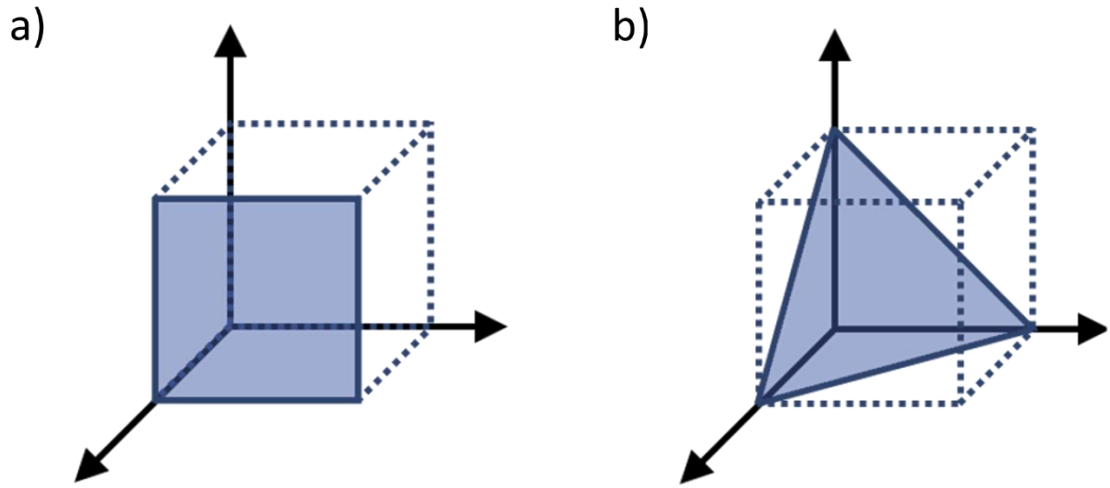


Figure 2: (a)  $\langle 100 \rangle$  plane and (b)  $\langle 111 \rangle$  plane. Figure modified from the original in [16].

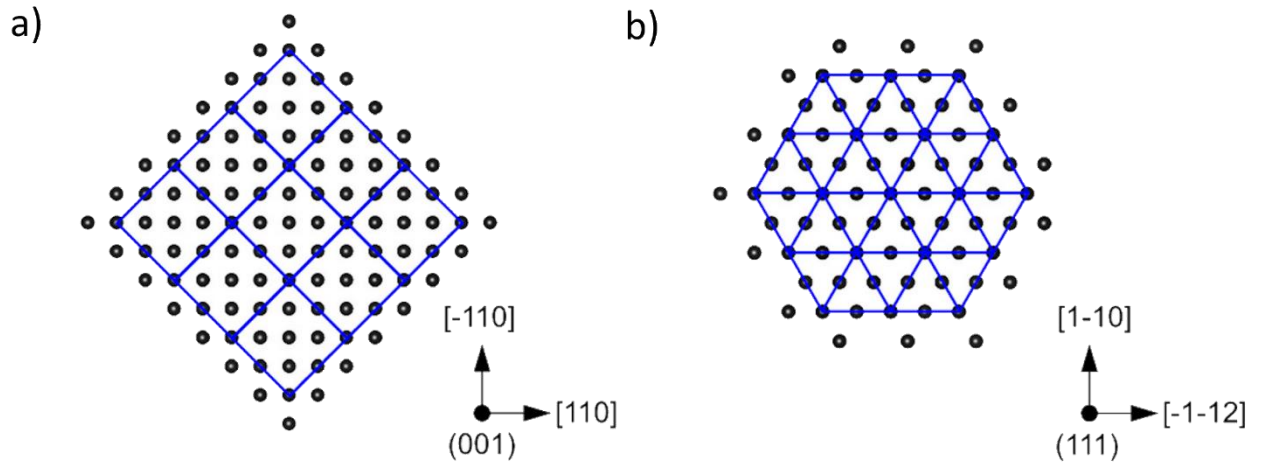
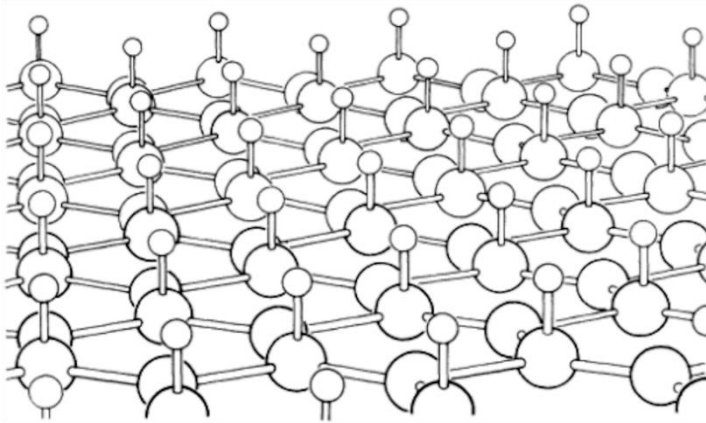


Figure 3: Atomic array of (a)  $\langle 100 \rangle$  diamonds, and (b)  $\langle 111 \rangle$  diamonds. Figures captured from [18].

a)



b)

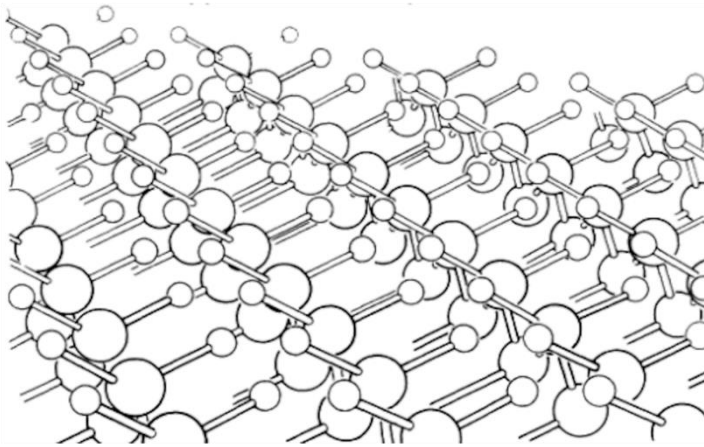


Figure 4: Schematic diagram of hydrogen-chemisorbed diamond surfaces in (a)  $\langle 111 \rangle$  orientation, and  $\langle 100 \rangle$  orientation. For  $\langle 111 \rangle$  face, an H-atom is adsorbed onto the surface pointing upwards. For  $\langle 100 \rangle$ , two H-atoms are sticking out from the surface. This creates a different surface environment and, hence, the surface activities between the  $\langle 111 \rangle$  and  $\langle 100 \rangle$  faces. Figure captured from [19].

In the case of semiconductors, the interaction between the crystal surface and the dopant atoms becomes crucial. Compared to the  $\langle 100 \rangle$  orientation,  $\langle 111 \rangle$  diamond films have a higher dopant incorporation efficiency.<sup>18, 20</sup> While the dopant atoms incorporate into the diamond structure, only a portion of them are located in sites for electrical activity. Kato *et al.* reported that the electrical activity of doped phosphorus in  $\langle 100 \rangle$  diamonds was around 10%, while it was around 70% for  $\langle 111 \rangle$  diamonds.<sup>21</sup>

### 4.3. Synthetic Diamond

With such a wide range of applications, studies have been conducted to find an optimal method for synthesising diamonds. An ideal synthetic method should be able to synthesise diamonds large in size so that they can be applied in different fields where a large crystal is required. Besides, the diamond formed should also be in single-crystalline form. Polycrystalline diamonds usually contain graphite-like structures at the grain boundaries, which would dampen the

superior properties of diamonds.<sup>3</sup> In nature, diamonds are found deep in the Earth's crust. The carbon forms very slowly hundreds of kilometres below the surface, where the temperature and pressure are very high, causing the carbon to crystallise into diamonds.<sup>22-23</sup>

#### **4.3.1. High-Pressure High-Temperature Method**

Diamonds have been commercially synthesised via the high-pressure high-temperature method (HPHT) for years. The method relies on applying extreme temperature and pressure (approximately 5-5.5 GPa and 1350-1450 °C) to a carbon source like graphite, with the presence of molten metals (e.g., Fe, Co and Ni). The carbon source dissolves in the heated metal flux, which supersaturates the solvent and recrystallises onto the existing seed crystals.<sup>24</sup> Under these conditions, the denser diamond structure becomes more thermodynamically favourable than the graphite structure, similar to natural diamonds.<sup>2, 8</sup>

HPHT has been the primary method for synthesising single-crystal diamonds as the crystal it formed has high quality. The dislocation densities for the diamond made by HPHT were reported as  $10^2$ - $10^4$  cm<sup>-2</sup>, which is much lower than that for other methods.<sup>18, 25</sup> However, the size of the crystal grown by HPHT is limited to a few millimetres due to the practical limitation of the anvil in the high-pressure system. Scientists had tried to put the seed crystals side by side, known as the 'mosaic method', but the crystals formed contained a high density of defects at the position where the boundaries of the seed crystals were located.<sup>18, 26, 27</sup> Besides, Tallaire *et al.* reported that the <111> crystal made from HPHT contained lots of nitrogen and metal impurities. Such crystal purity would be unfavourable for most electronic applications.<sup>20</sup>

#### **4.3.2. Chemical Vapour Deposition**

An alternative method for synthesising diamond is known as chemical vapour deposition (CVD). The process involves a gas-phase chemical reaction followed by carbon deposition onto the surface of a solid substrate (*Fig. 5*).<sup>28</sup>

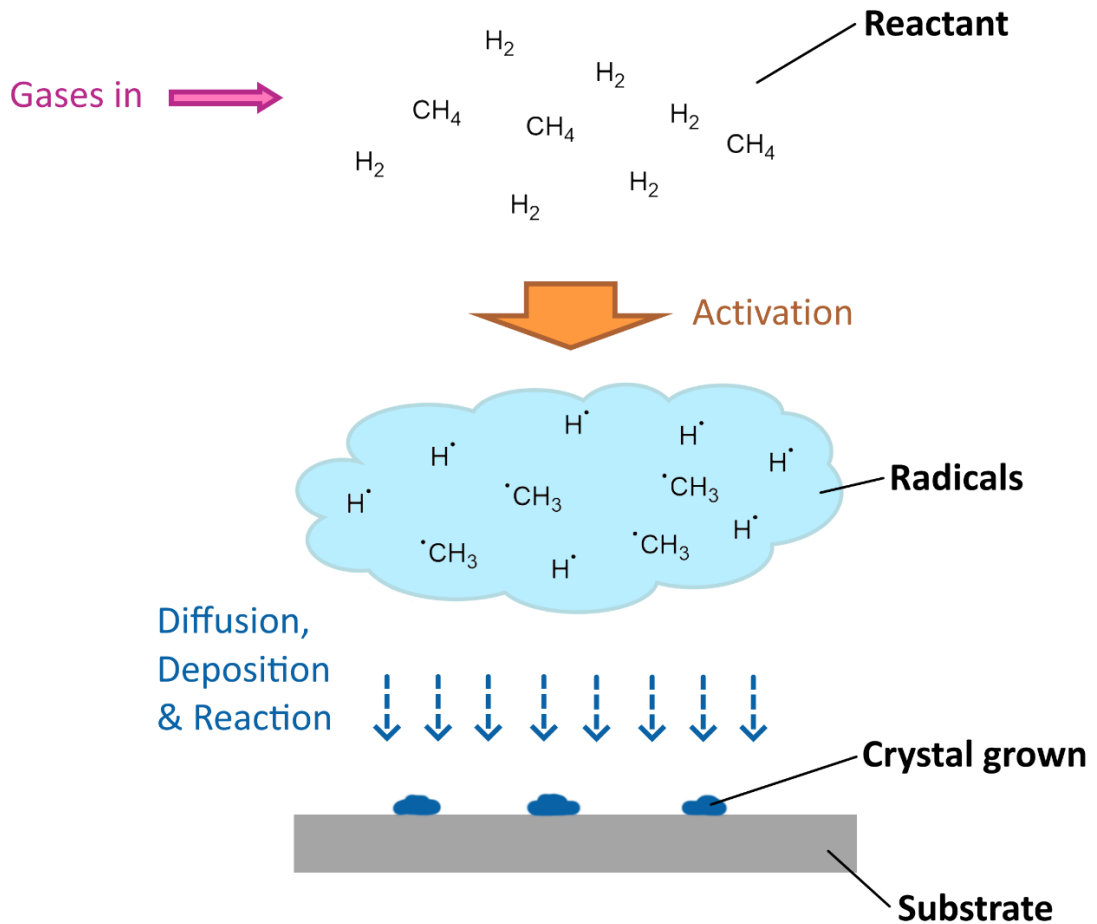


Figure 5: A schematic diagram of the general process of chemical vapour deposition. The reactant gas is assumed to be CH<sub>4</sub>/H<sub>2</sub>. Upon activation, the reactant gases become radicals, which then diffuse and deposit onto the substrate. Diamond crystals are grown after surface chemical reactions. Diagram recreated and modified from the original in [28].

#### 4.3.2.1. General Chemical Mechanism

In CVD, a gaseous carbon-containing precursor (e.g., CH<sub>4</sub>) is pumped into the reactor chamber with excess hydrogen gas (typically 1-2% by volume). The gas mixture is activated and forms H and CH<sub>3</sub> radicals. The two radicals gradually diffuse and adsorbed onto the substrate surface. The H radicals are responsible for etching the hydrogen atoms on the surface of the crystal lattice, which creates a reactive site on the crystal structure. The CH<sub>3</sub> radical then attacks the site, creating a dangling methyl group. The process repeats until one dangling methyl group is adjacent to a dangling methyl radical. The radical then attacks the methyl group and closes the structure. The diamond lattice is then enlarged (Fig. 6).<sup>2</sup>

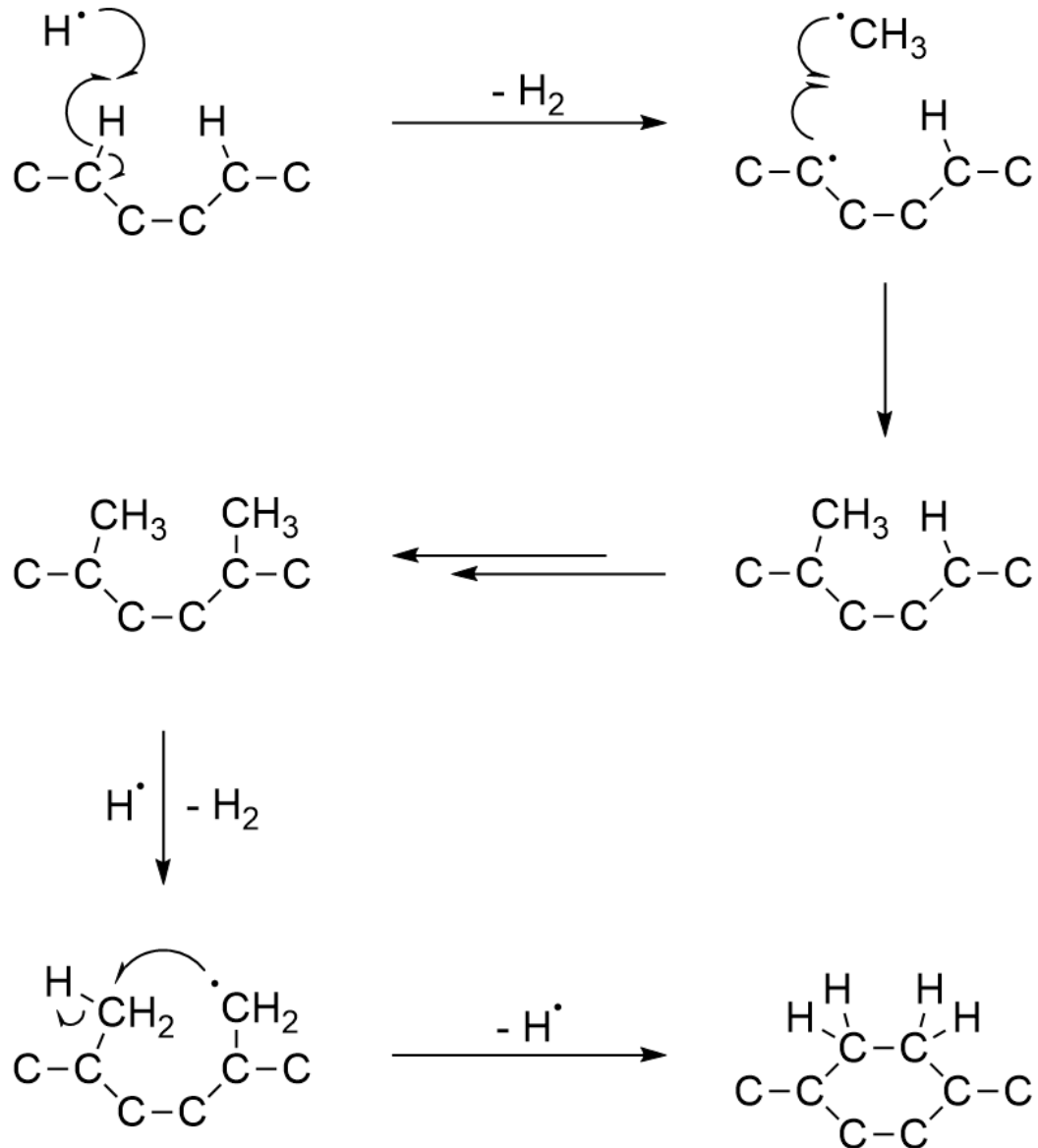


Figure 6: Simplified chemical mechanism of diamond growth in CVD. All the steps are reversible. Figure recreated and modified from [2].

#### 4.3.2.2. Gas Activation

The gas mixture can be activated by various means. For example, it can be excited by simply heating it with hot filaments (HF-CVD). A common alternative is plasma activation using D.C. current or microwaves.<sup>2</sup> All these methods share a similar chemical mechanism mentioned previously.

When searching for an optimal method for synthetic diamond production, the growth rate becomes an important factor in deciding which method to use. Compared to hot filament or microwave plasma activation, D.C. glow discharge plasma gives a much higher diamond growth rate.<sup>29,30</sup> Having the current pulsed also prevents the cathode from overheating, which would potentially un-stabilise the plasma by creating unwanted arc discharge.<sup>31</sup>

#### 4.3.2.3. Choice of substrate

The CVD method enables the possibility of heteroepitaxial growth of diamonds, in which the diamond is grown on a different material.<sup>32</sup> In a homoepitaxial diamond growth process, the diamond grows on existing diamond seeds, follows the  $sp^3$  structure and extends it.<sup>33</sup> Substrates with similar lattice structures should be used to achieve a similar effect but in a heteroepitaxial way.<sup>18, 26</sup> This can be achieved by abrading the surface of the substrate into similar lattice structures. However, the method would damage the lattice and create a rough surface, which might result in random growth directions.<sup>33</sup> The substrate should, therefore, inherently have a similar lattice structure as diamonds. Among all the materials, iridium has the most similar atomic array pattern to diamonds, which makes it a good substrate candidate (Fig. 7).<sup>26, 33</sup>

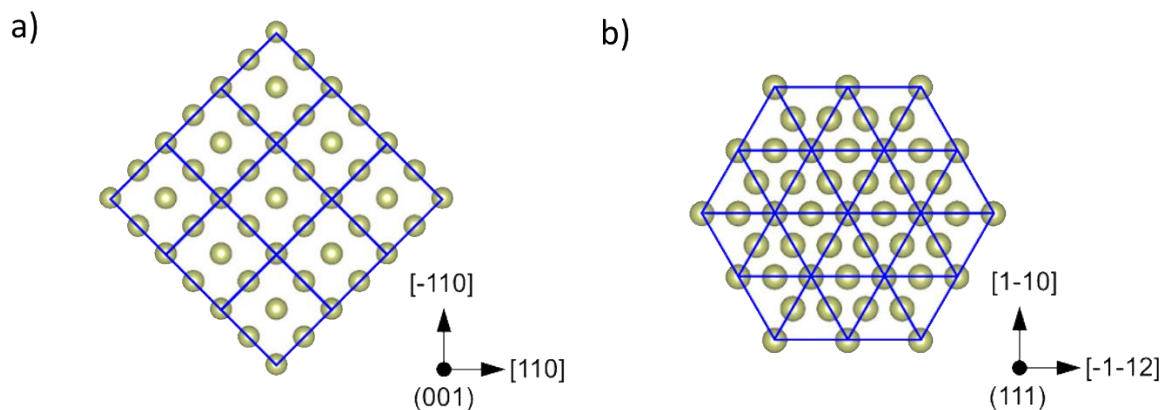


Figure 7: Atomic arrays of (a)  $\langle 100 \rangle$  iridium, and (b)  $\langle 111 \rangle$  iridium. Figure captured from [18].

Iridium is not readily available in large sizes, but it can be coated onto another large substrate, such as sapphire, MgO or YSZ (yttria-stabilised zirconia)/Si. Among all the materials, sapphire stands out due to its low cost and a small thermal coefficient of thermal expansion. In addition, large sapphires are readily available. Hence, Ir/sapphire is a common substrate used in CVD diamonds.<sup>18, 26, 33</sup>

### 4.4. Spectroscopic Methods

#### 4.4.1. Raman Spectroscopy

Raman spectroscopy is a useful technique for understanding the chemical and structural compositions of the sample at micron and sub-micron sizes.<sup>34</sup> The technique relies on measuring the energy of the scattered laser photon, which gives an energy shift compared to the incident photon after colliding with the sample's electron density. Materials with different chemical and structural compositions interact with the photon in different ways. When the scattered laser is detected, it gives a spectral band that depends on the molecular compositions. This forms the basis of the spectroscopic technique (Fig. 8).<sup>35</sup>

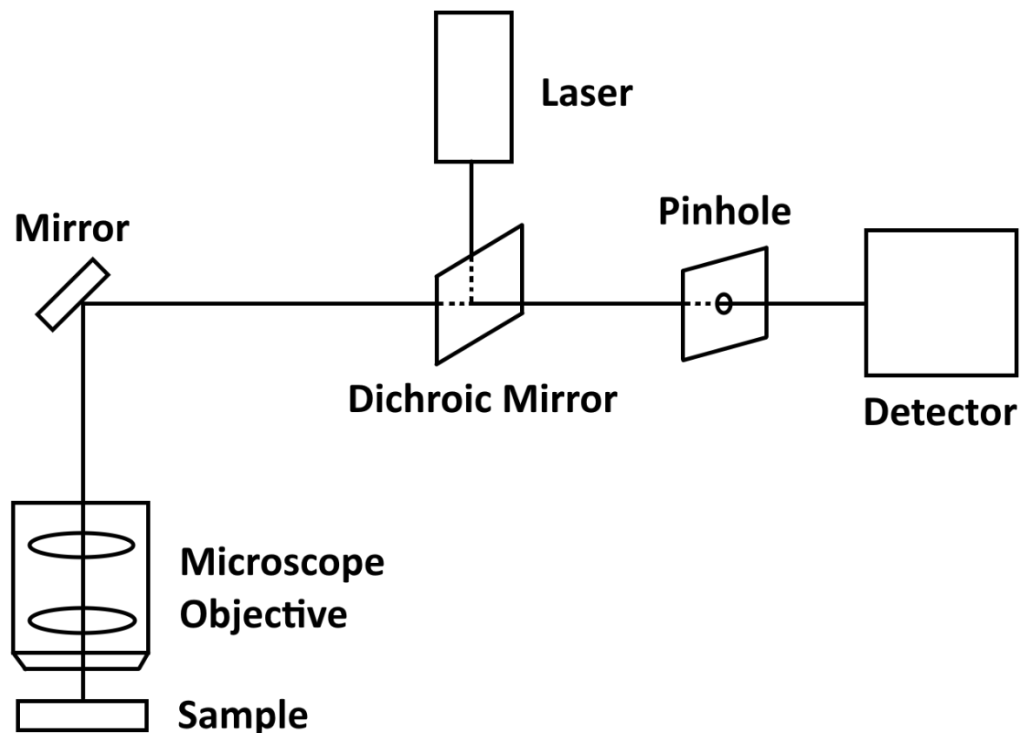


Figure 8: A simplified schematic diagram of a confocal Raman microscope. The laser is focused onto the sample via the microscope objectives. The laser photons interact with the electron densities in the sample and are inelastically scattered back through the dichroic mirror. The scattered laser photons eventually get detected by the detector. A spectrum can be produced by placing a diffraction grating before the detector. This forms the basis of the confocal Raman spectroscopy. Figure recreated and modified from [36].

The Raman spectrum of a pure diamond shows a sharp peak at around  $1332\text{ cm}^{-1}$ , while the graphitic region is around  $1580\text{ cm}^{-1}$ .<sup>37</sup> The characteristics of these two peaks allow the identification of the composition of the film deposited onto the substrate.

#### 4.4.2. Scanning Tunneling Microscopy/Atomic Force Spectroscopy

Scanning tunnelling microscopy (STM) is a technique that allows the characterisation of the surface. When the tip is very close to the surface, the electron density of the tip and the surface starts to overlap. Upon applying a voltage, the electrons tunnel from one side to another, creating a tunnelling current, which is very sensitive to the surface topography.<sup>38</sup> The technique can be operated in two different modes while scanning across the surface. Constant height mode measures the topography based on the change of the distance-dependent tunnelling current. Constant current mode is measured by moving the probe's sharp tip up and down on the surface, keeping the tunnelling current constant.<sup>39</sup>

Atomic force spectroscopy (AFM) is a similar technique, but instead of relying on quantum tunnelling of the electrons, the probe tip moves upon experiencing forces on the sample surface. The deflection of the probe is detected using a laser and a photodetector. Hence, the technique can also give very detailed topographic information.<sup>40</sup>

#### 4.4.3. X-Ray Diffraction

X-ray diffraction (XRD) can be used to understand the lattice structure of a crystalline material. The X-ray is diffracted into specific diffraction patterns based on the structure's crystallinity and atomic arrangement. XRD provides no information on the chemical composition of the crystal lattice, but it can be used to identify useful information, including the crystallinity, lattice structure and crystal orientation. <sup>41, 42</sup>

#### 4.4.4. Scanning Electron Microscopy

Scanning electron microscopy (SEM) relies on the inelastic collision of the electrons with the sample's atoms. The electrons are guided by electromagnetic lenses and raster the substrate surface, and the secondary electrons produced are detected to form an SEM image. <sup>43</sup>

SEM is a useful tool for revealing the orientation of the crystal due to the difference in the atomic arrays between the two lattice faces. The SEM image of  $\langle 100 \rangle$  diamonds shows cubic-like crystals, while that of  $\langle 111 \rangle$  diamonds shows triangular faceted surfaces (Fig. 9). <sup>44</sup>

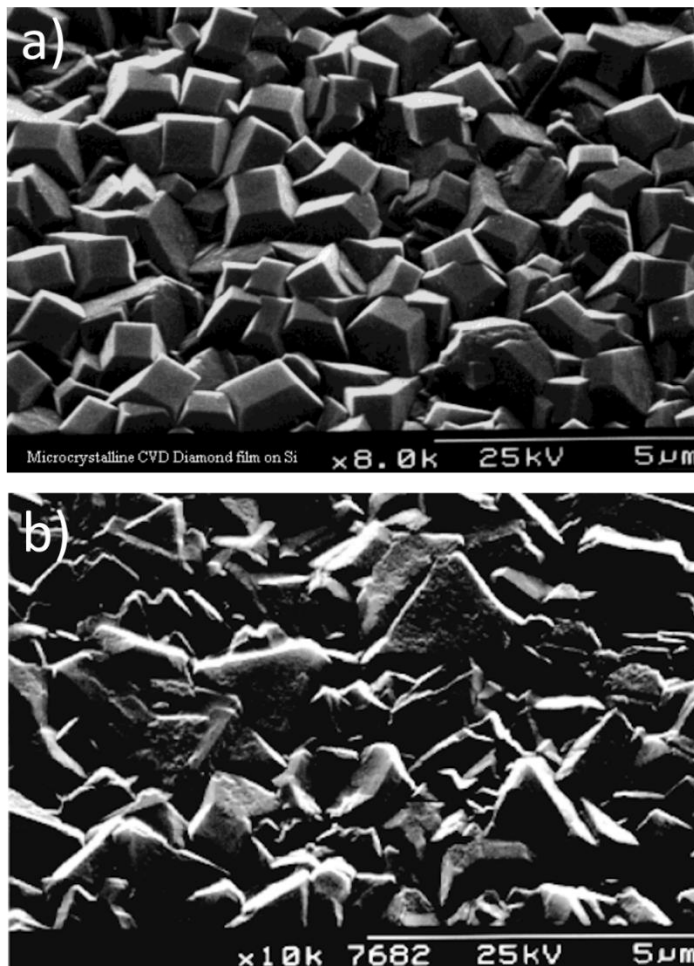


Figure 9: SEM images of (a)  $\langle 100 \rangle$  diamond crystals, and (b)  $\langle 111 \rangle$  diamond crystals. The  $\langle 100 \rangle$  crystals were in cubic-like shapes, while the surfaces of the  $\langle 111 \rangle$  crystals appeared to be triangular. Images taken by the University of Bristol CVD Diamond Group. <sup>44</sup>

#### 4.4.5. Optical Emission Spectroscopy

Optical emission spectroscopy (OES) is a technique for analysing plasma composition by detecting the light emitted from the plasma.<sup>45</sup> Such techniques allow the analysis to be carried out in real-time with the chemical reaction without disturbing the reaction itself.

Liang *et al.* reported an increase in the C<sub>2</sub> emission intensity at a higher CVD diamond growth rate.<sup>46</sup> At a pressure of around 200 Torr, three of the C<sub>2</sub> peaks (471.55, 516.52 and 563.25 nm) were reported to have a magnitude 7 times more than the others. The wavelengths also corresponded to a greenish visible colour, which can also be seen during the reaction.<sup>47</sup> These provide a good indicator of the reaction condition inside the chamber, which could be adjusted by changing the gas concentration.<sup>48</sup>

#### 4.5. Project Details

In this project, we conducted two pulsed-DC CVD reactions, one using molybdenum as the substrate and one using iridium-coated sapphire (Ir/sapphire). The first molybdenum reaction served as a 'trial run'. By analysing the product from the molybdenum reaction, the reaction condition can be adjusted for the second CVD reaction, which used Ir/sapphire, an ideal substrate combination, as mentioned before.

We also investigated the possibility of growing diamonds at low CH<sub>4</sub> concentrations using pulsed-DC CVD. Typically, HF-CVD is able to grow diamonds at a very low CH<sub>4</sub> concentration (less than 1% CH<sub>4</sub> in H<sub>2</sub>).<sup>49, 50</sup> On the other hand, DC-CVD typically grows diamonds at a slightly higher concentration (ca. 1-4% CH<sub>4</sub> in H<sub>2</sub>). However, the quality of the diamond films was reported to be better at lower CH<sub>4</sub> content, with predominantly <111> lattice orientations at around 1% of CH<sub>4</sub>.<sup>51, 52</sup> In our project, we tried to lower the CH<sub>4</sub> concentration inside the chamber to 1.5% during the reaction with Ir/sapphire substrate.

Here, we reported the results obtained from the Raman spectroscopy of the products in both reactions and the OES result from the Ir/sapphire reaction. Due to significant project delays, we were not able to carry out any other spectroscopic measurements in time. It would be ideal to analyse the product in more detail using methods like AFM, SEM, and XRD.

### 5. Experimental

#### 5.1. CVD Diamond on Molybdenum

Before the reaction, the two copper electrodes of the CVD reactor (Balzers Coating System, see *Fig. 10, 11* and *12*) were aligned in the centre to each other so that the surfaces of the two rods were parallel. The inter-electrode spacing was set to 20 mm. A molybdenum substrate (25 mm in diameter) was placed onto the anode (*Fig. 13*). A mask was put onto the Mo substrate (with a 1 cm × 1 cm square hole at the centre and two 6.8 mm × 3.3 mm rectangular holes on two sides). The reactor was then sealed and vacuumed.



Figure 10: A photo of the Balzers CVD Coating System.

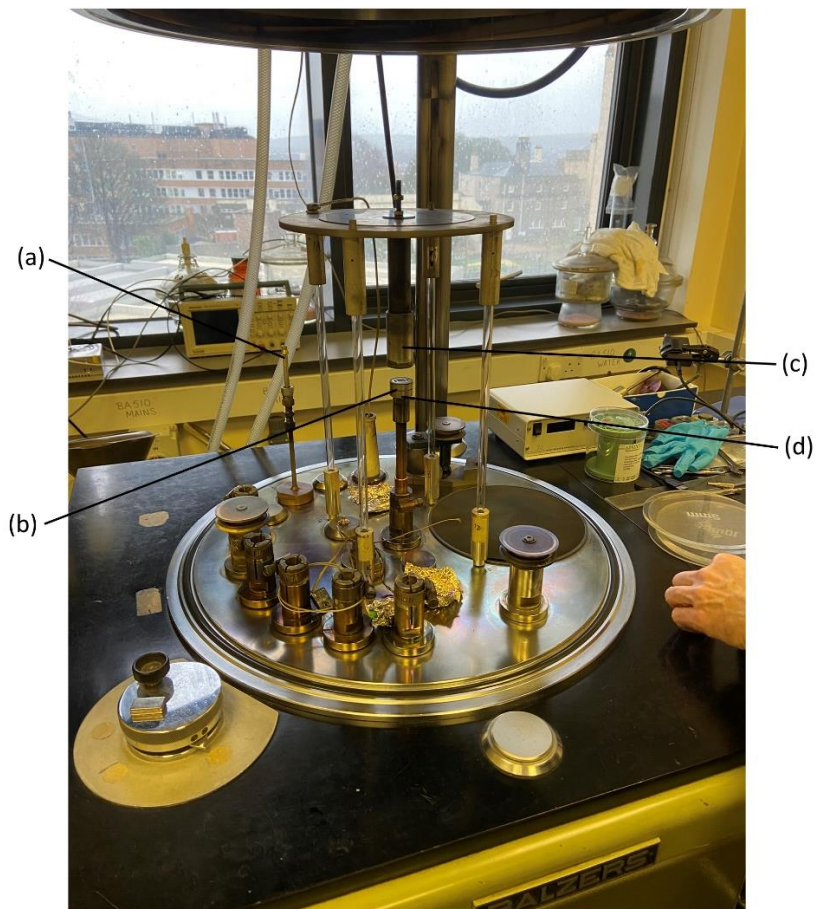


Figure 11: A photo of the internals of the Balzers CVD Coating System, with the major components labelled: (a) gas input, (b) substrate, (c) cathode, (d) anode.

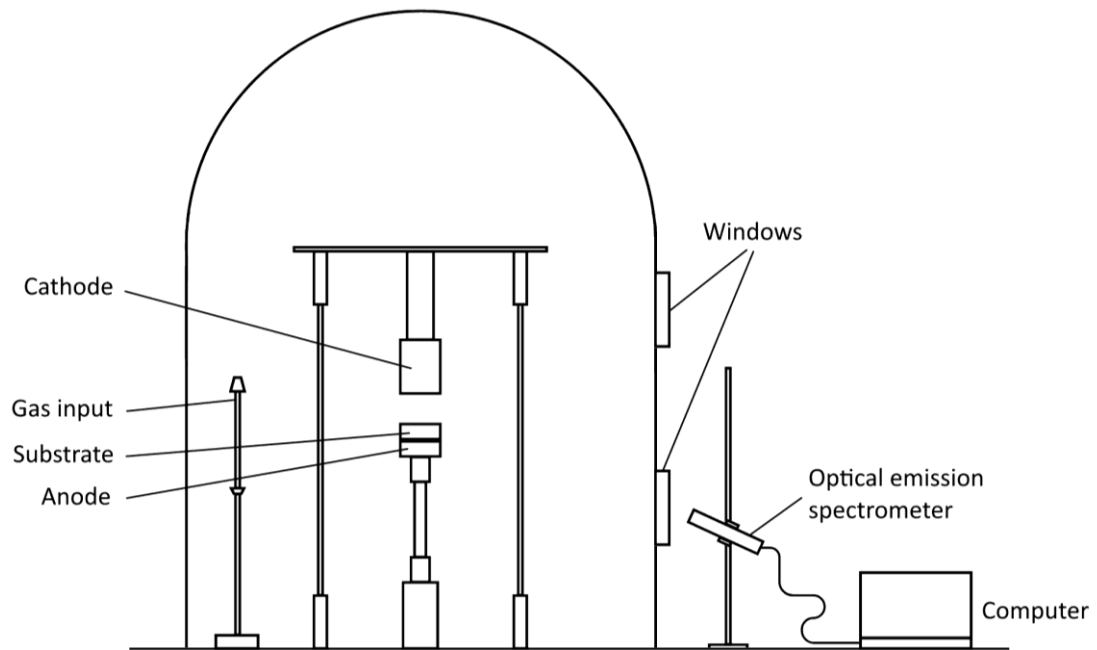


Figure 12: A simplified schematic diagram of the Balzers CVD Coating System. Note that the optical emission spectrometer and the computer were not set up for the molybdenum reaction.



Figure 13: A close-up photo of the set-up for the molybdenum reaction. A molybdenum substrate was placed on top of the anode. A mask was placed on top of the substrate, allowing the reaction to occur only at the square hole and the two small rectangular holes on both sides.

A steady flux of CH<sub>4</sub> (12.5 SCCM, 2.5%) in H<sub>2</sub> was pumped into the chamber. The power was increased gradually from 500 W to 1200 W while the pressure was reaching 150.0 Torr. The chamber was then switched to 'static mode', in which the input flux of gas was stopped, and the chamber was sealed. The content inside the chamber was allowed to react for 1 hour. During the reaction, the temperature of the cathode, plasma and substrate was measured using an infra-red thermometer (Minolta/Land Cyclops 52 Thermometer, as shown in Fig. 14). After the reaction, the power of the electrodes was switched off to let the content cool down. The product substrate was obtained after venting the chamber.



Figure 14: A photo of the Minolta infra-red thermometer, which was used to measure the temperature of the cathode, plasma and substrate.

## 5.2. CVD Diamond on Iridium/sapphire

A Balzers CVD coating machine was used to grow diamonds on Ir/sapphire. Before the reaction, the two electrodes were placed centred to each other so that the two electrode surfaces were in parallel. The inter-electrode gaps were set to 22 mm. A molybdenum disc (25 mm in diameter and 5 mm in thickness) was placed onto the anode, with an Ir/sapphire chip (6.8 mm × 3.3 mm in dimension, 100 nm in thickness of the Ir layer) on top (see Fig. 15).

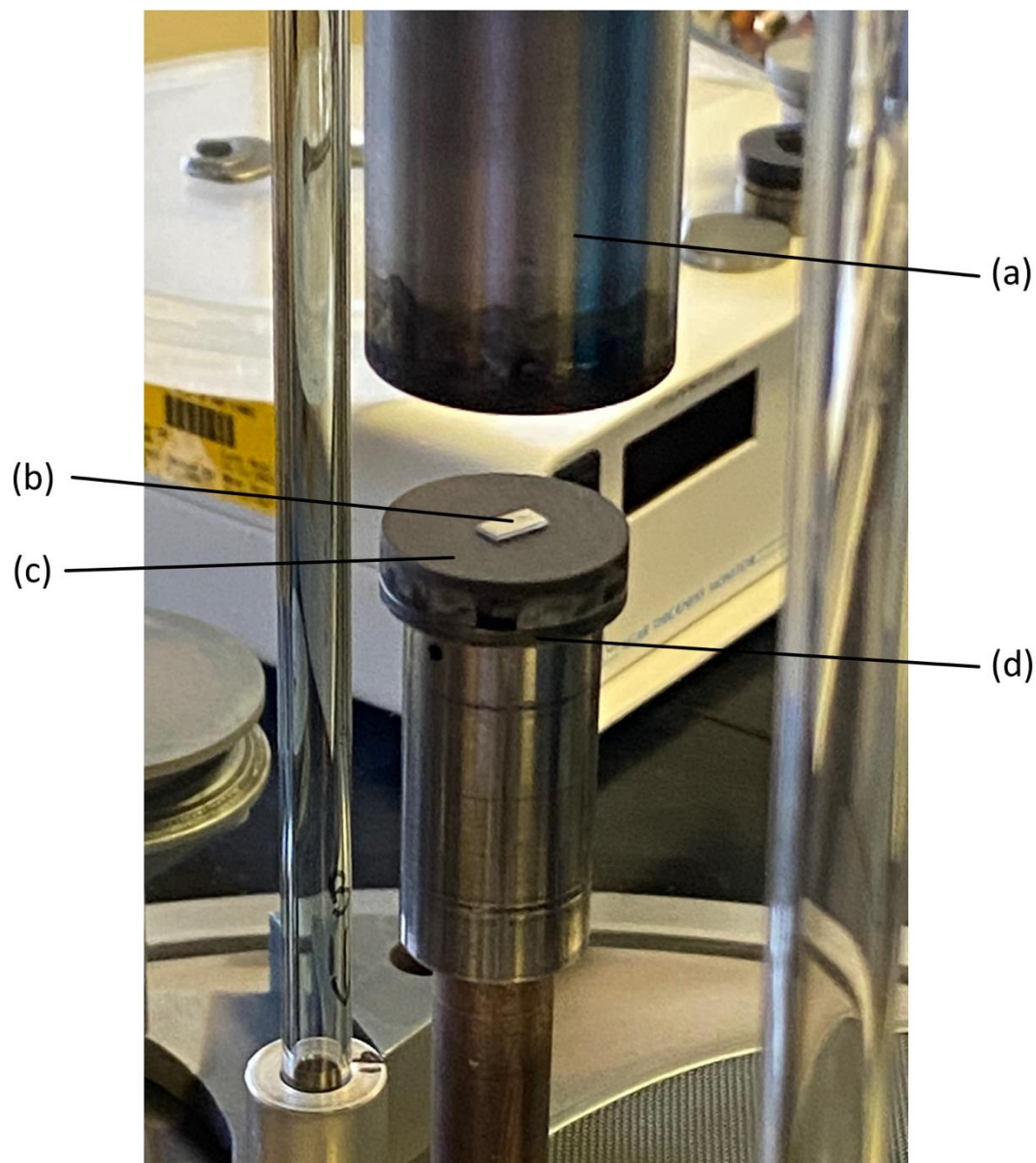


Figure 15: A close-up photo of the set-up for the Ir/sapphire reaction, with the major components labelled: (a) cathode, (b) Ir/sapphire chip, (c) molybdenum substrate, (d) anode. The photo was taken after the reaction. Hence, the surface of the substrate was grey-black in colour due to the deposition of carbon.

To set up a starting condition, the reaction chamber was sealed and vacuumed (ca. 0.01 Torr). The power of the electrodes was set to 500 W. A steady flow of H<sub>2</sub> gas (600 SCCM) was then pumped into the chamber for 10 min. When the internal pressure reached 42.4 Torr, the chamber was vacuumed again (ca. 0.01 Torr) and ready for reaction.

A steady stream of CH<sub>4</sub> (7.5 SCCM, 1.5%) in H<sub>2</sub> (500 SCCM) was pumped into the reactor. As the internal pressure increased, the power of the electrodes was gradually increased from 500 W to 1000 W when the pressure reached 150.3 Torr.

The reactor was then switched to 'static mode', allowing the content to react for 1 hour. During the reaction, the temperature of the cathode, the plasma and the substrate was measured using the Minolta infra-red thermometer. The power of the electrodes was then switched off to allow the content to cool down. The product substrate was obtained from the chamber after venting the content inside.

### 5.3. Optical Emission Spectroscopy

During the CVD reaction with Ir/sapphire, an optical emission spectrometer (Broadcom Spectrometer Qmini) was set up next to the reactor's lower window (see Fig. 12). The spectrometer was connected to a computer, which was used to display and analyse the spectra in the spectroscopy software Waves (by Broadcom). The spectrometer was adjusted to point directly to the plasma inside the chamber and measure the light produced by the plasma (Fig. 16).

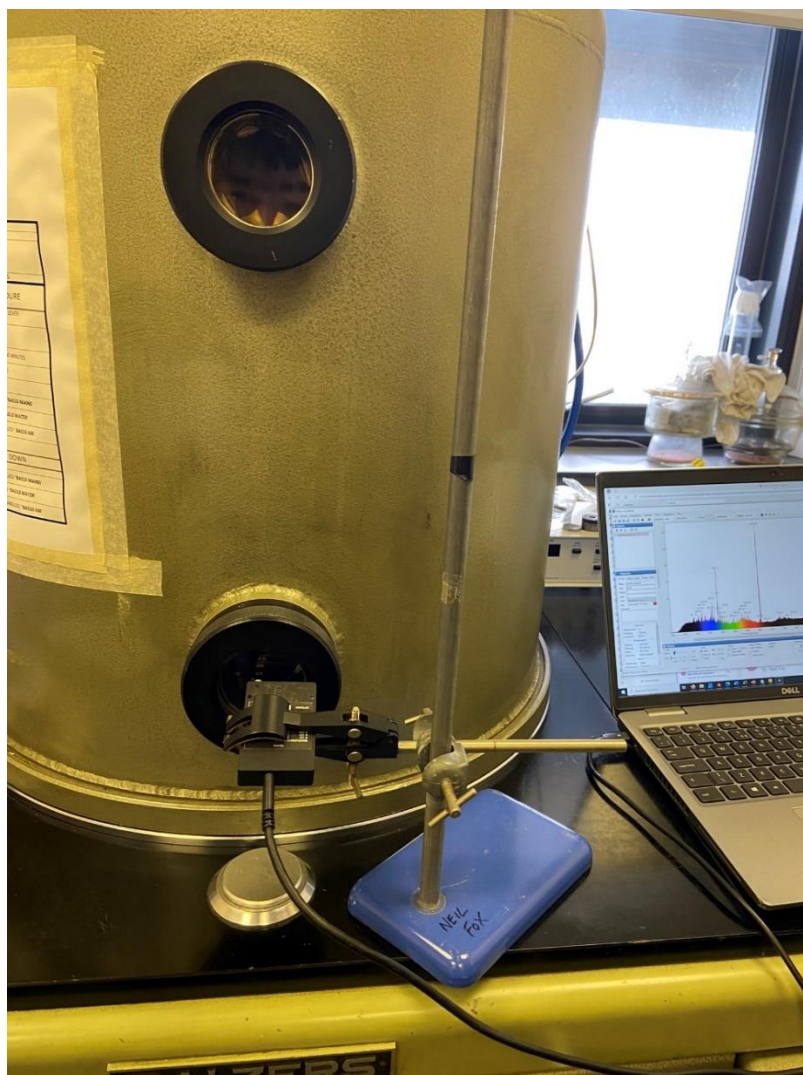


Figure 16: A photo of the OES set-up during the CVD reaction with Ir/sapphire substrate. The spectrometer was held by the clamp and stand, pointing towards the plasma inside the reactor. The spectrometer was connected to the laptop, which had the analysing software displaying the OES spectrum in real time.

## 5.4. Raman Spectroscopy

Several Raman spectroscopies were done on the products from both CVD reactions. The spectrum was obtained from the Raman system (Renishaw Raman System with LEICA DM LM confocal microscope, with a diffraction grating of  $1200 \text{ lines mm}^{-1}$  for the laser), as shown in *Fig. 17*. A diamond piece was used to calibrate the Raman system beforehand, producing a sharp diamond  $1332 \text{ cm}^{-1}$  peak.<sup>37</sup> The wavelength of the laser was set to  $514 \text{ nm}$ , which was a green laser. The spectra were analysed using the software WiRE 2.0, with the spectral resolution being  $0.5 \text{ cm}^{-1}$ .



*Figure 17: A photo of the Renishaw Raman spectrometer, with LEICA confocal microscope installed.*

## 6. Result & Discussion

### 6.1. Diamond Grown on Molybdenum and Ir/sapphire

Before inspecting the product samples with Raman spectroscopy, a diamond piece was used to calibrate the Raman system (*Fig. 18*). The spectrum shows a single, sharp peak at  $1331.78 \text{ cm}^{-1}$ , which is approximately close to the literature value ( $1332 \text{ cm}^{-1}$ ).<sup>37</sup>

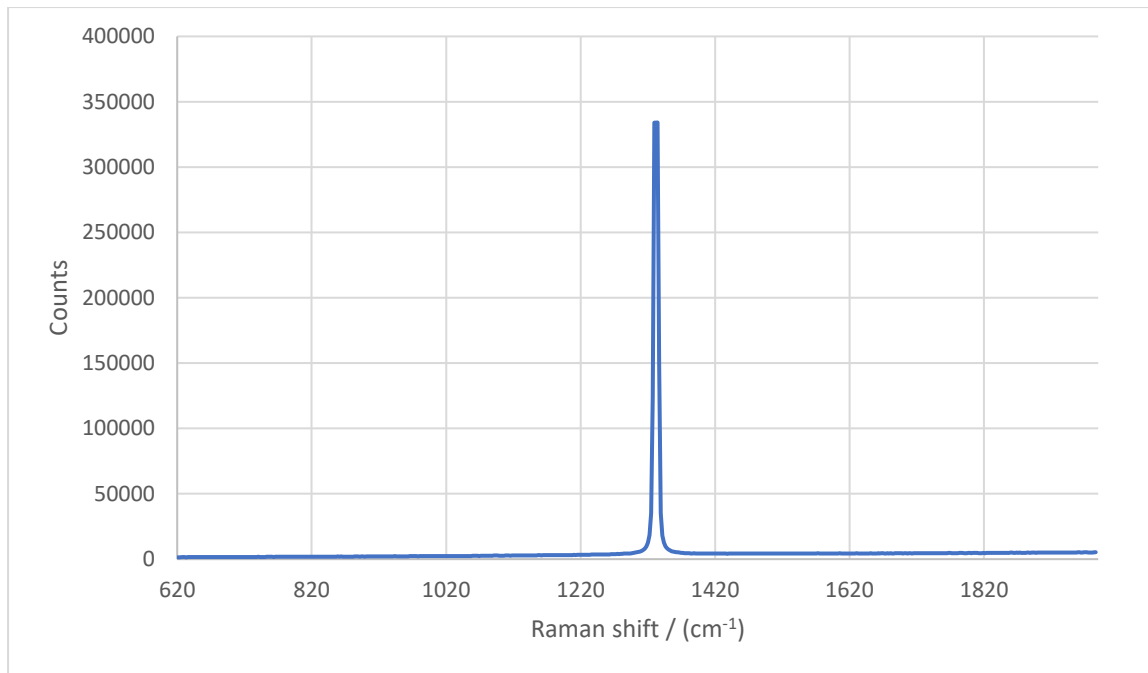


Figure 18: Raman spectrum of the calibrating diamond piece. Raman shift of the peak:  $1331.78 \text{ cm}^{-1}$ .

In the CVD reaction with Mo substrate, the carbon was deposited onto the substrate according to the shape of the mask, resulting in a square and two rectangular marks on the surface (Fig. 19). The centre square was significantly dark in colour, which looked like a relatively high portion of graphitic compositions. For each 'mark', Raman spectroscopy was done at both the centre and the periphery area. Table 1 recorded the Raman shift of the significant peak around the diamond region. The full Raman spectra of all the regions can be found in Appendix 1.

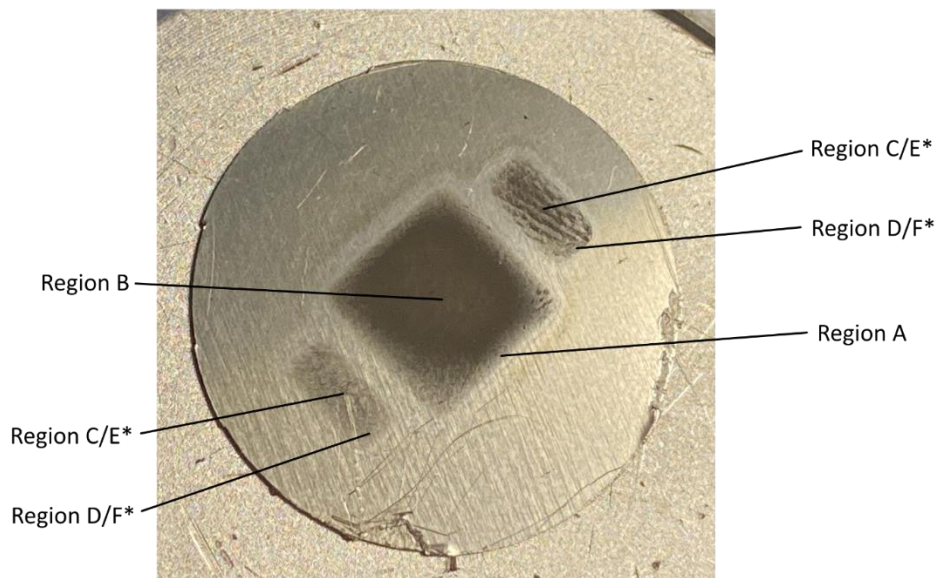


Figure 19: A photo of the Mo substrate after the CVD reaction. A grey square mark can be seen at the centre of the disc, with two rectangular marks on the side. The periphery and the centre of the square were labelled as Region A and B, respectively. The centre of the two rectangular marks was Region C and E, while the periphery was Region D and F. (\*It was unclear which rectangular mark corresponded to Region C or E, and the same for the periphery regions D and F.)

Table 1: Raman shifts of the film on the Mo substrate at various positions of the disc, following the labels in Fig. 19.

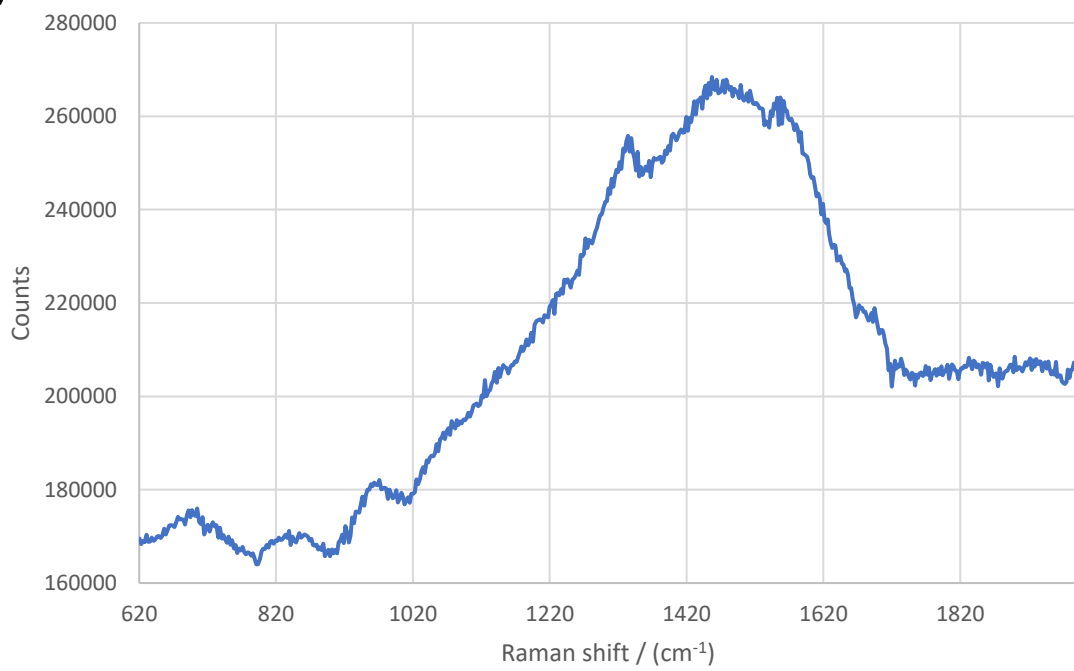
	Raman shift / (cm <sup>-1</sup> )
Region A	1335.37
Region B	1332.44
Region C	1338.71
Region D	1332.44
Region E	1334.52
Region F	1334.78

The result from Raman spectroscopy suggested that diamonds had successfully grown in all regions to a certain extent. Some values were slightly higher than the literature value of 1332 cm<sup>-1</sup>. This might be due to the stress of the crystalline structure, which could be caused by the formation of lower-density graphitic carbon.<sup>53</sup> From the Raman spectrum of Region B, the Raman peaks were much stronger in the graphitic region than near the diamond region (Fig. 20b). This might suggest that a relatively high portion of graphitic crystal structures formed in the square box, which explains the darker appearance of the film. For the rectangular film, although the crystal densities were lower than the square film (as shown in Fig. 20a and Fig. 20c), they gave more distinct diamond peaks in the spectrum (Fig. 20d). This suggested that the crystal quality was better in the rectangular box than in the square box in this CVD reaction.

a)



b)



c)

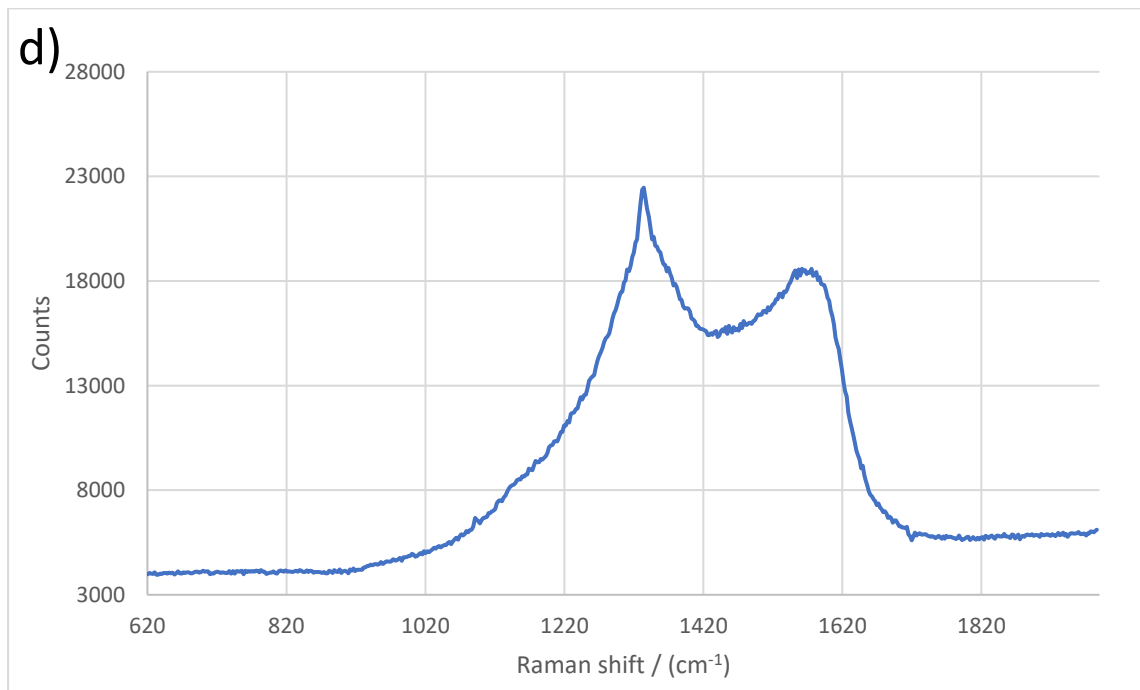
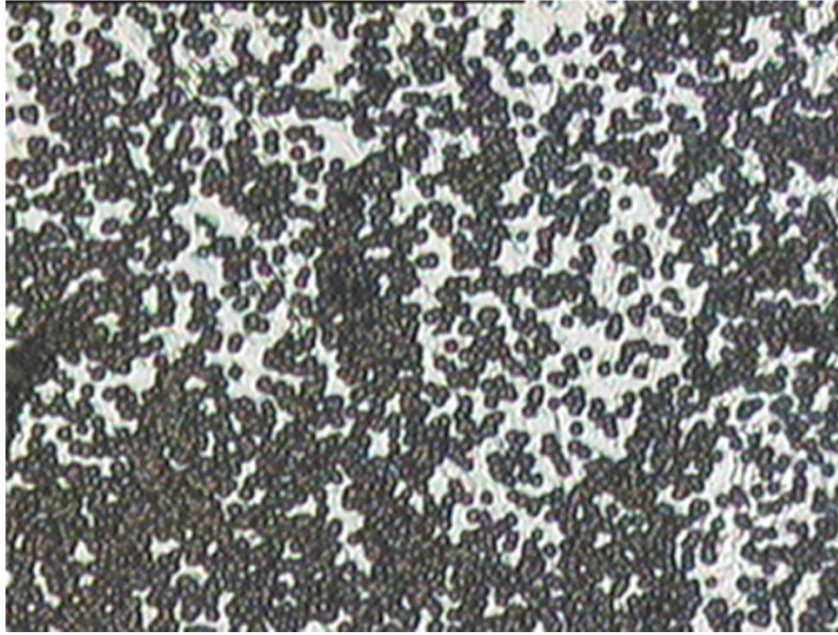
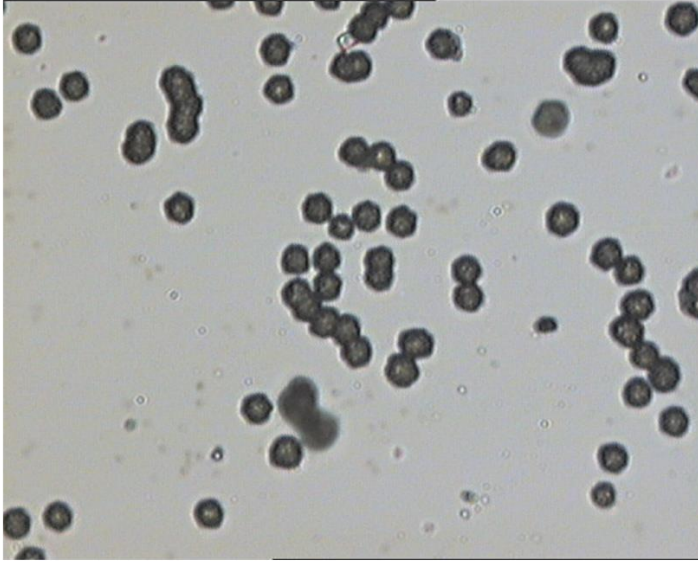


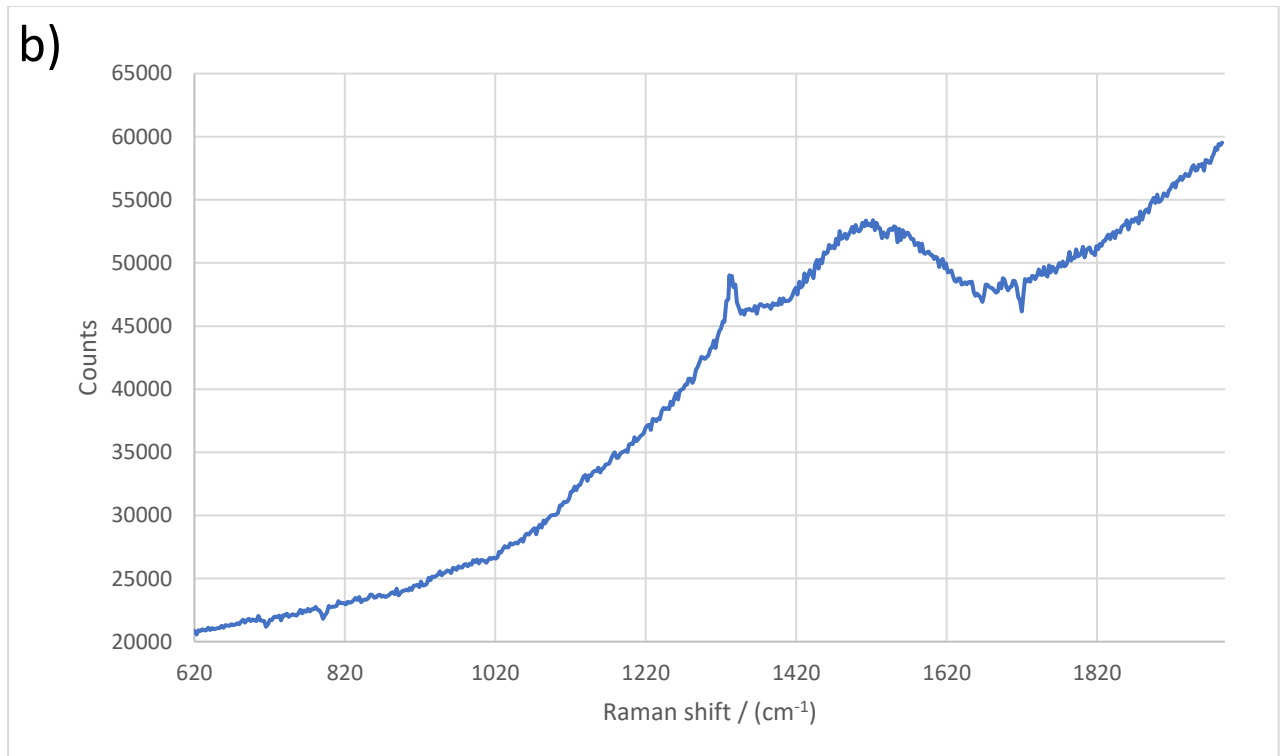
Figure 20: (a) Screenshot of the live video of Raman spectroscopy at Region B. (b) Raman spectrum at Region B (Raman shift of the peak:  $1332.44 \text{ cm}^{-1}$ ). (c) Screenshot of the live video of Raman spectroscopy at Region D. (d) Raman spectrum at Region D (Raman shift of the peak:  $1332.44 \text{ cm}^{-1}$ ). From the Raman spectrum, the square film in the middle of the substrate contained a significant portion of graphitic structures compared to the rectangular film on the side.

Based on the result, in our second CVD reaction, we used Ir/sapphire substrates of the same size as the rectangular hole of the mask in the first CVD reaction. Similar to before, Raman spectroscopy was done at the centre and periphery of the Ir/sapphire chips (Fig. 21).

a)



b)



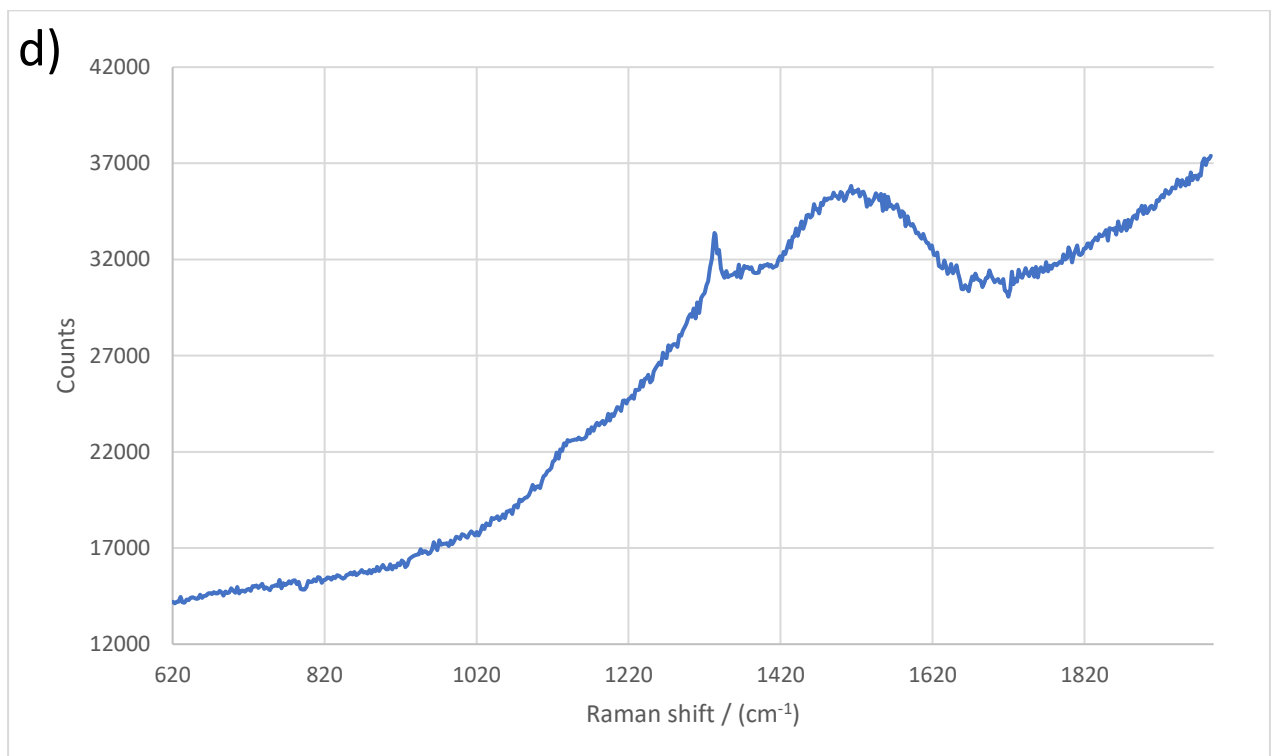
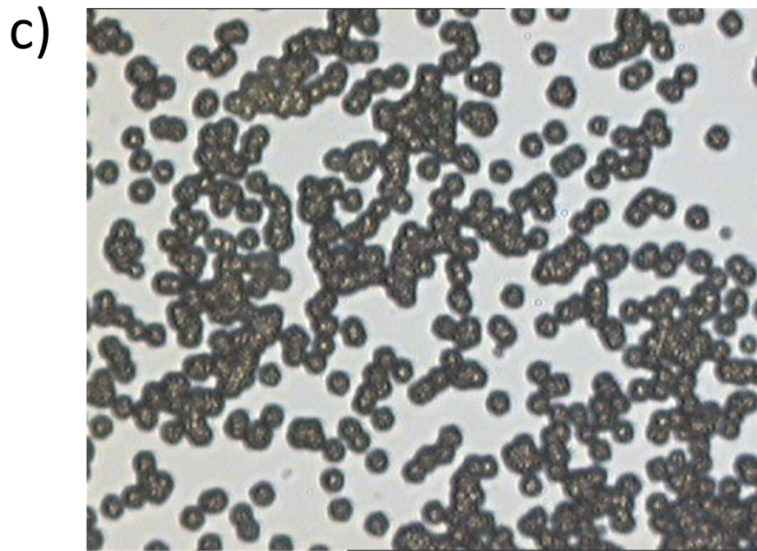


Figure 21: (a) Screenshot of the live video of Raman spectroscopy at the centre of the Ir/sapphire substrate. (b) Raman spectrum of the film at the centre of the Ir/sapphire substrate (Raman shift of the peak:  $1333.61\text{ cm}^{-1}$ ). (c) Screenshot of the live video of Raman spectroscopy at the periphery region of the Ir/sapphire substrate. (d) Raman spectrum of the film at the periphery region of the Ir/sapphire substrate (Raman shift of the peak:  $1333.22\text{ cm}^{-1}$ ).

In both Raman spectra, a sharper, narrower peak appears (compared to the Raman spectra of the film on the Mo substrate). The peak also shifts less away from the literature diamond peak. This might suggest that the crystal experienced less compressive stress from any formation of graphitic structure.<sup>53</sup>

The diamond crystals were grown in larger clusters at the periphery than the centre, as shown in Figures 21a and 21c. The crystal particles have an average size of  $6.16 \pm 0.087\ \mu\text{m}$  (Fig. 22) and were grown throughout the Ir/sapphire chip. This is a promising result for future CVD diamond

growth, considering the reaction was done heteroepitaxially without seeding (*i.e.*, no pre-existing diamond seeds were placed on the substrate for growth).

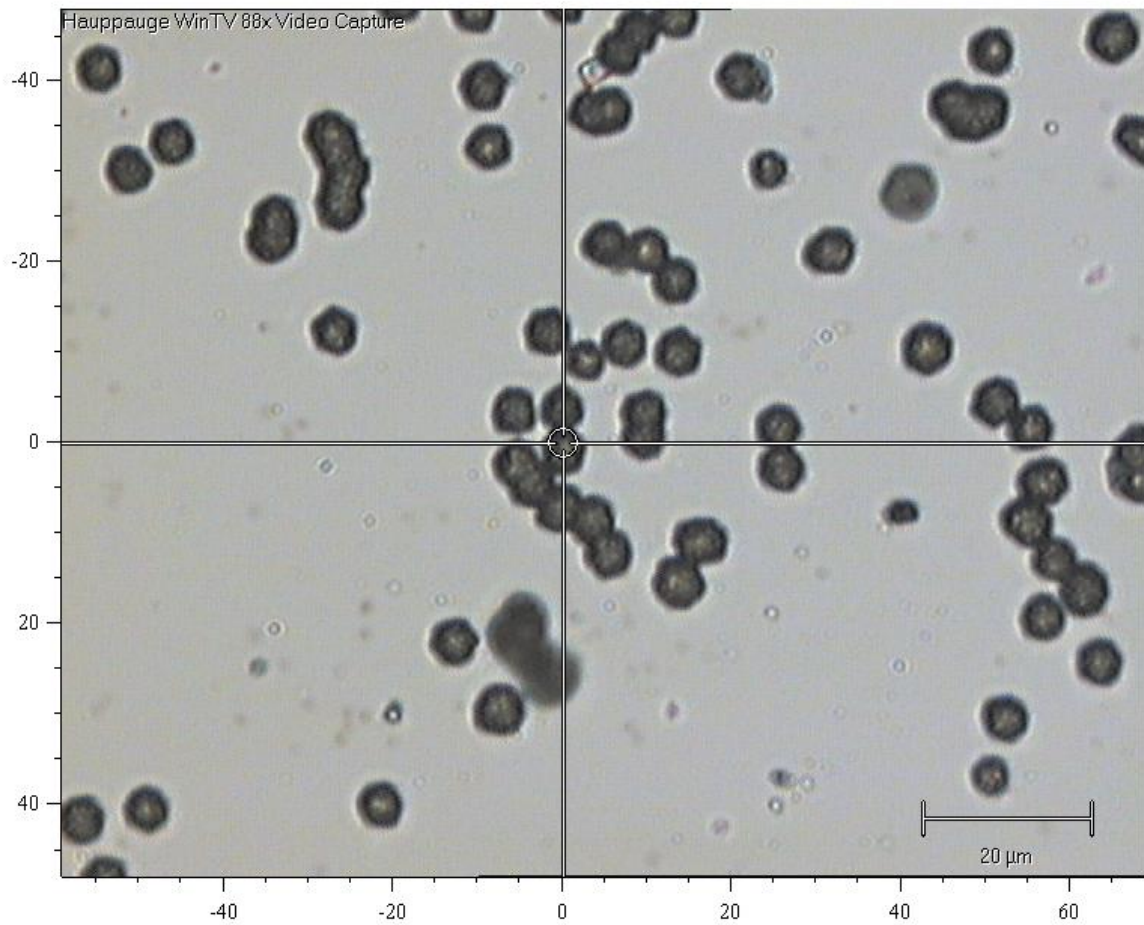


Figure 22: A screenshot of the spectroscopy software, with the scale of the photo in the bottom-right corner.

One of the differences between the two CVD runs was the temperature. In the first CVD run, the power of the electrode was set to 1200 W. However, it was believed that the substrate became too hot and potentially graphitised the film on the substrate.<sup>53</sup> In the second CVD run, the power of the electrodes was set to a lower value of 1000 W instead of 1200 W, and a lower temperature was measured in the second CVD (see Table 2).

Table 2: The temperature of the cathode ( $T_{cathode}$ ), plasma ( $T_{plasma}$ ), and substrates ( $T_{substrate}$ ) during the first CVD (Mo substrate) and the second CVD (Ir/sapphire substrate). The temperature was measured using a Minolta thermometer.

	$T_{cathode} / (^{\circ}\text{C})$	$T_{plasma} / (^{\circ}\text{C})$	$T_{substrate} / (^{\circ}\text{C})$
1 <sup>st</sup> CVD	1090	800	1110
2 <sup>nd</sup> CVD	1010	680	850

These suggested that the CVD reaction had grown diamonds of relatively better quality than the film on the Mo substrate. However, more detailed structural microscopy would be required to confirm the results. For example, XRD might be useful in identifying the orientation of the crystal grown, and SEM or AFM might be useful in studying surface topography.

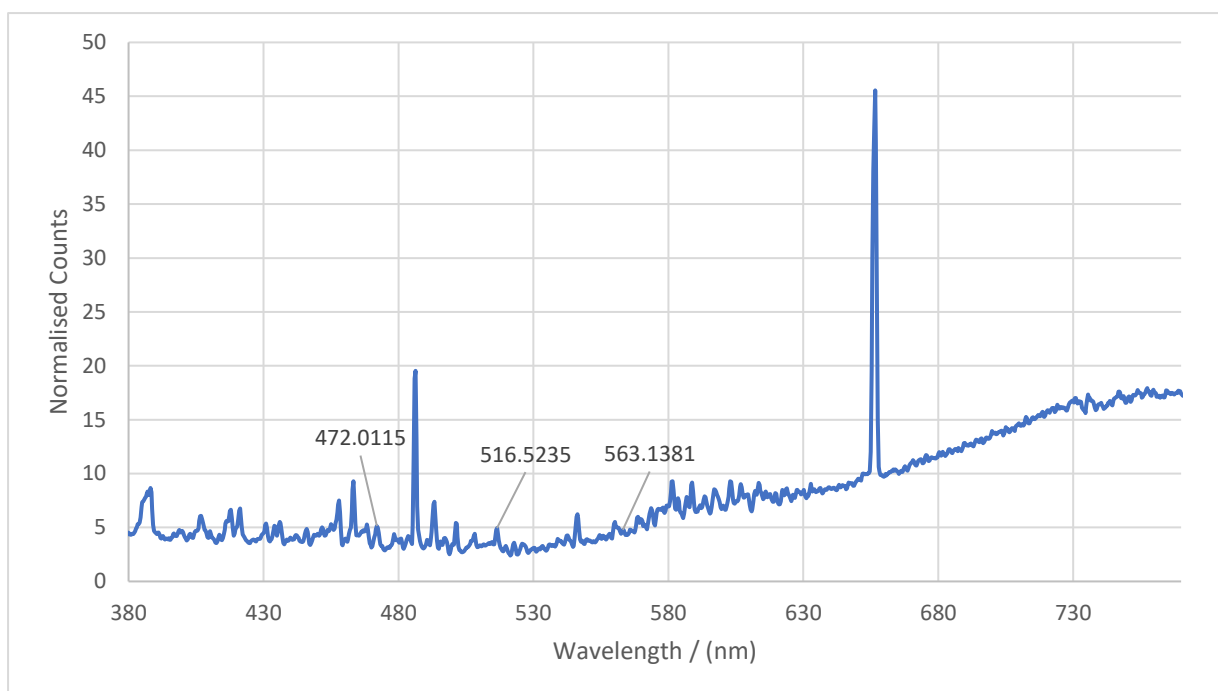


Figure 23: Optical emission spectrum captured during the CVD reaction with Ir/sapphire substrate. The three  $C_2$  peaks appeared but were weaker than Hemawan *et al.* reported. The figure here displays the spectrum within the visible light wavelength range (380 nm to 770 nm).<sup>54</sup> The full spectrum can be found in Appendix 3.

In the optical emission spectrum, the three  $C_2$  peaks appeared, but not as intense as Hemawan *et al.* reported (Fig. 23).<sup>47</sup> It is worth mentioning that there was no visible greenish plasma during the Ir/sapphire CVD run, but a yellowish plasma line was seen during the molybdenum run (Fig. 24).

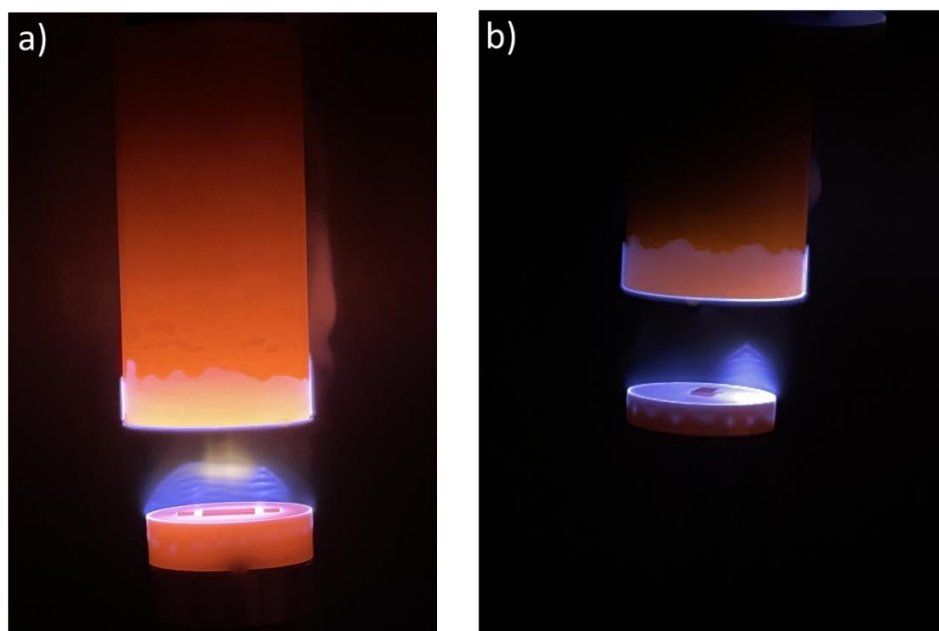
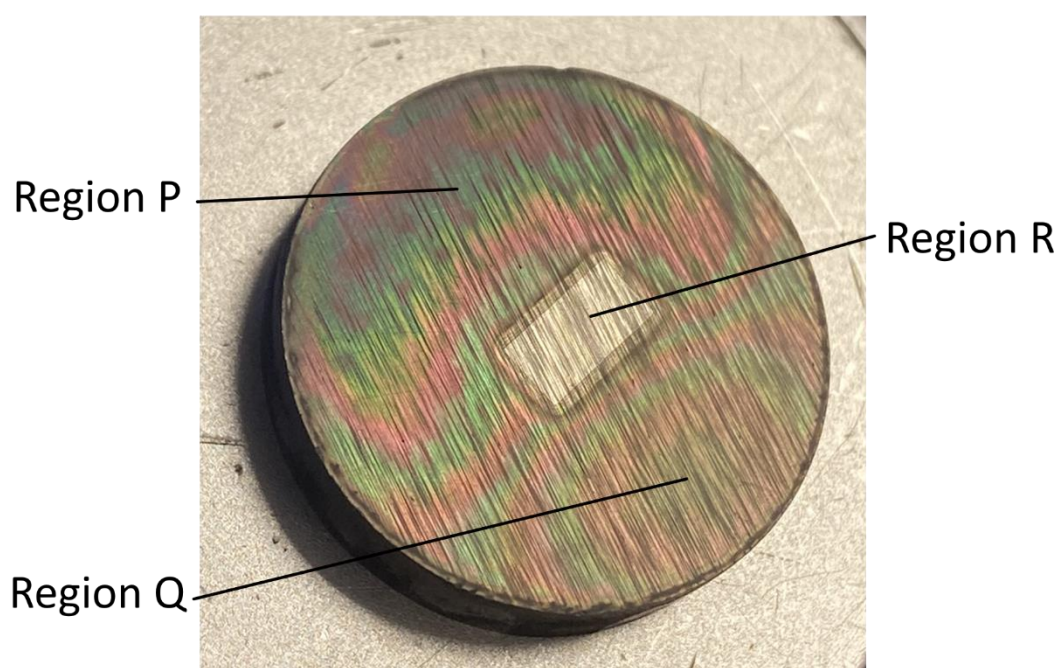


Figure 24: Lines of plasma appeared in (a) the first CVD reaction with Mo substrate), and (b) the second CVD reaction with Ir/sapphire substrate. In the first CVD reaction, some yellowish-green plasma lines could be clearly seen, but the colour disappeared a while later. In the second CVD reaction, no yellowish or greenish plasma was observed. Also, the plasma lines were located on one side of the substrate, covering approximately 40% of the surface of the Mo disc.

However, to study the correlation between certain reaction conditions and the diamond growth rate, more than a single OES result is required, and further continuous, time-dependent experiments would be required. It is also possible to nucleate the diamond on Ir/sapphire using DC-CVD and compare the growth rate in various CVD methods.

## 6.2. Graphite Film on Molybdenum Disc

After the second CVD reaction, the surface of the molybdenum disc (that was used to support the Ir/sapphire chip) became iridescent (*Fig. 25*). Iridescence is a phenomenon resulting from film interference. When light strikes a thin layer, the incident light is reflected by the upper and lower boundaries of the film. The two reflected waves interfere with each other, creating a coloured appearance that changes with respect to the observer or illumination direction. <sup>55, 56</sup>



*Figure 25: A photo of the Mo disc after the CVD reaction with Ir/sapphire substrate. Region P corresponds to the side of the disc with a strong iridescent effect. Region Q corresponds to the opposite side of the disc, where the effect of iridescence is weaker. This is also where the plasma line was located during the CVD reaction (see Fig. 24). Region R corresponds to the rectangular area where the Ir/sapphire chip was placed.*

Several Raman spectroscopies were done to understand the composition of the surface layer. From the spectra in *Fig. 26*, the surface layer was mainly composed of graphitic structures. There was no significant diamond peak. This suggested that the carbon was selectively deposited onto the Ir/sapphire instead of the molybdenum surface.

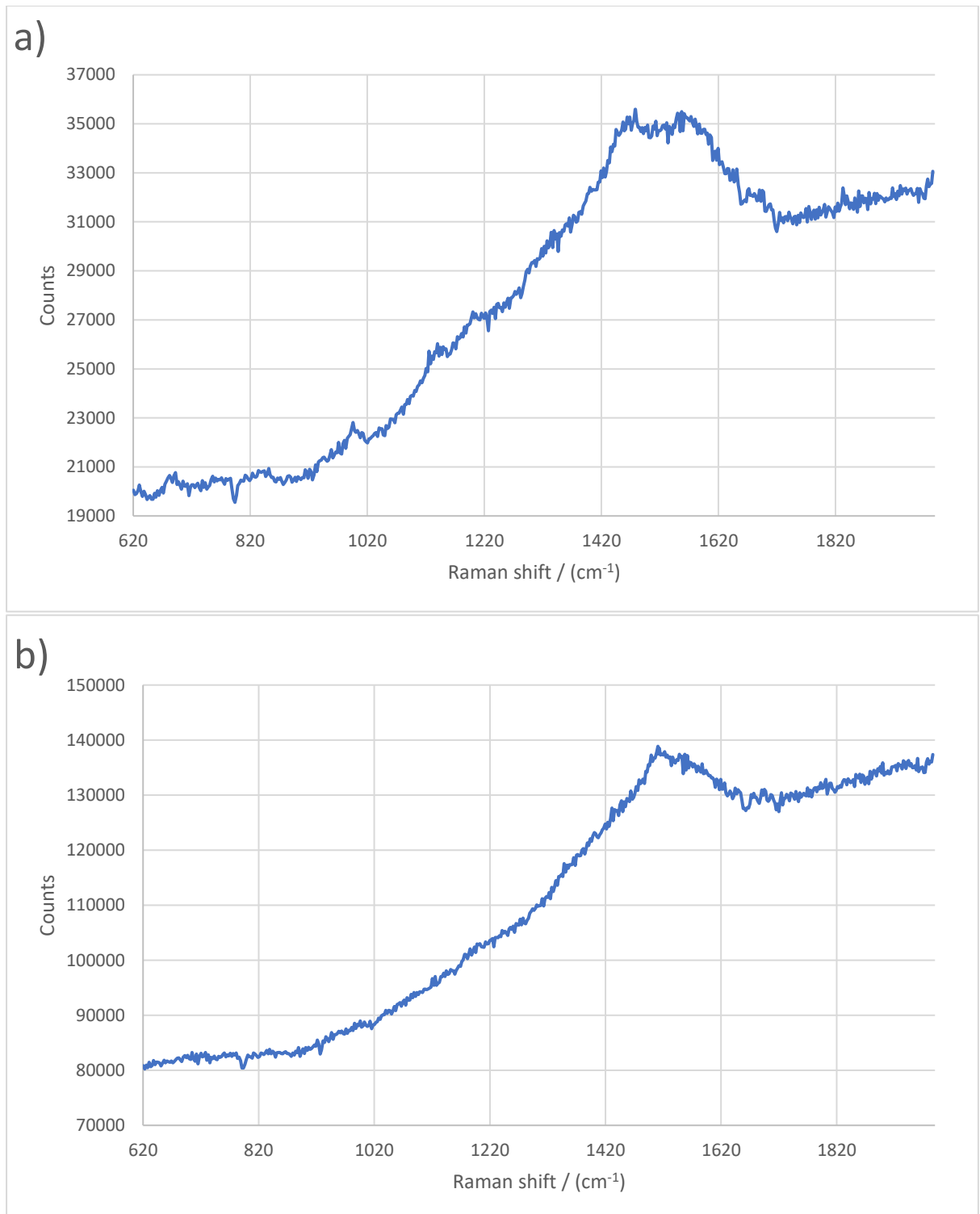


Figure 26: Raman spectra of the surface layer of the Mo substrate after the CVD reaction with Ir/sapphire at (a) Region P and (b) Region Q.

The Raman spectrum of Region R looks similar to a spectrum of just molybdenum (Fig. 27). This suggests that there was no deposition onto the rectangular area, which was covered by the Ir/sapphire chip. However, scratches can be seen across the whole Mo disc after the reaction, including Region R (see Fig. 25).

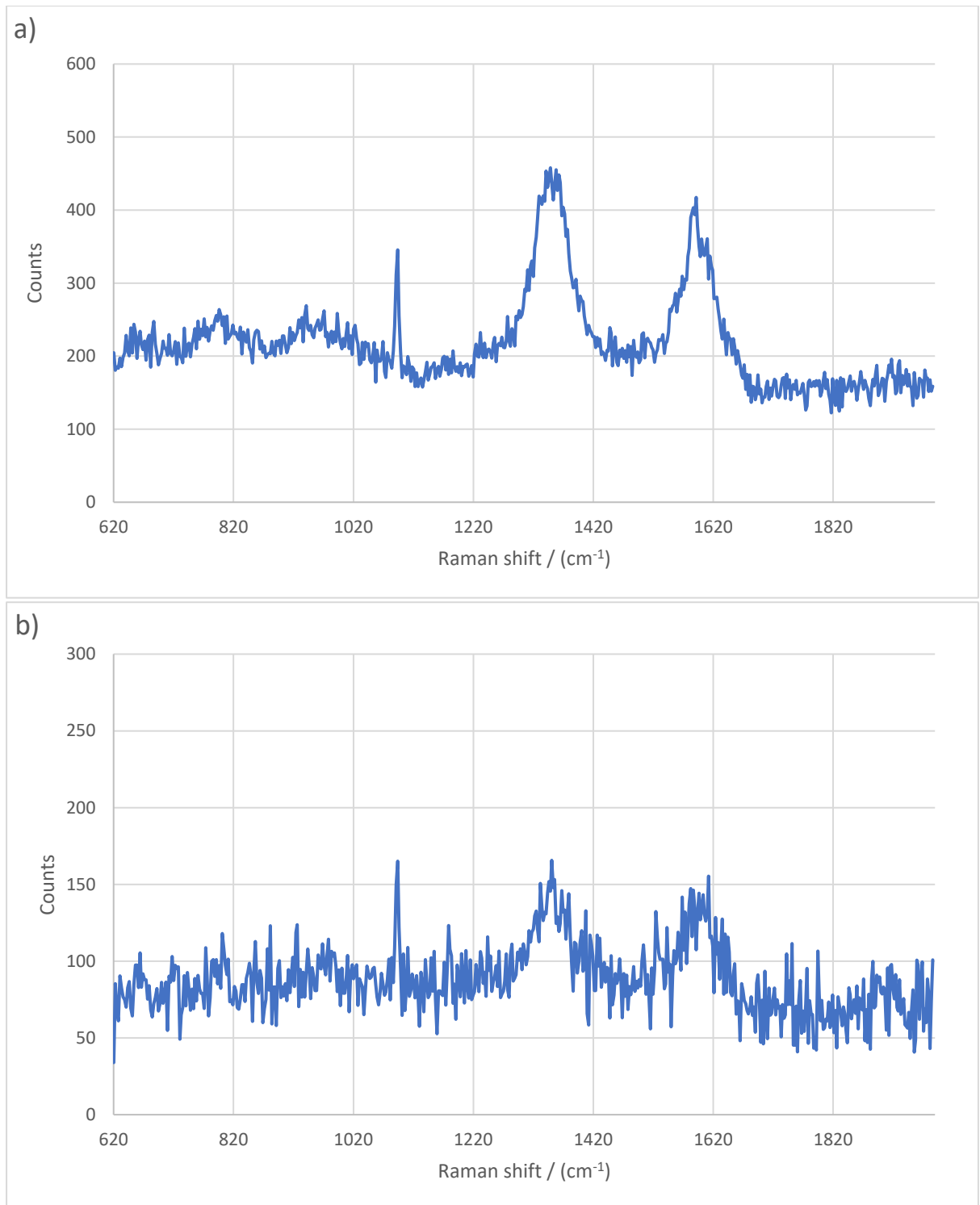


Figure 27: Raman spectra of (a) a molybdenum disc with no deposited layer on top and (b) Region R. The two spectra resemble a similar shape, suggesting that there was no deposited layer in Region R.

The iridescent appearance suggests that one or more thin layers of graphitic structures have formed on the Mo substrate alongside the diamond growing on the Ir/sapphire substrate. The experimental results provided a possibility of creating iridescent carbon layers, which might be helpful in optical applications or coloured coatings. It also offered a possibility of multi-synthesis of carbon layers, with the structure selectively on one substrate over the other. However,

further experiments are required to confirm the layers' structure and composition. Besides, more studies are needed to investigate whether the results are consistent and reproducible.

## 7. Conclusion

Using the DC-CVD reactor, we successfully grew diamond crystals on a heteroepitaxial layer without seedings. The process was carried out in a low methane concentration, which was reported to favour the formation of <111> diamond crystals. The Raman spectroscopy data agreed with the literature result of Ir/sapphire being the more ideal substrate candidate than molybdenum. Also, proceeding with the reaction at a lower temperature allowed the film to grow diamond crystals instead of graphitic compositions. The iridescent appearance of the molybdenum disc suggests the possible formation of thin layers of graphitic structures while diamonds were growing on the Ir/sapphire substrate simultaneously.

Given that the diamond crystal was grown without seeding, DC-CVD provides a good method for diamond nucleation. It is uncertain whether a longer reaction time would give rise to a large, thin layer of single-crystal diamond. However, the nucleated diamond can be further grown into polycrystalline diamond layers using other CVD methods (e.g. microwave CVD).

Due to practical limitations, further experiments and spectroscopic measurements were not able to be carried out in time. More detailed microscopies would be required to confirm the structure of the diamond crystals or the film layers on the substrates. For example, XRD might be useful in identifying the orientation of the crystal grown, and SEM or AFM might be useful in studying surface topography. Further research and experiments are also required to search for the optimal growing conditions for DC-CVD diamonds. For instance, the effect of growth time, electrodes' power or the temperature of the reaction environment on the growth rate and morphology of the diamond crystal.

## 8. Reference

- <sup>1</sup> A. Mainwood, M. E. Newton and M. Stoneham, *J. Phys.: Condens. Matter*, 2009, **21**, 360301.
- <sup>2</sup> M. N. R. Ashfold, P. W. May, C. A. Rego and N. M. Everitt, *Chem. Soc. Rev.*, 1994, **23**, 21-30.
- <sup>3</sup> P. W. May, *Science*, 2008, **319**, 1490-1491.
- <sup>4</sup> N. Yang, S. Yu, J. V. Macpherson, Y. Einaga, H. Zhao, G. Zhao, G. M. Swain and X. Jiang, *Chem. Soc. Rev.*, 2019, **48**, 157-204.
- <sup>5</sup> M. H. Wong, O. Bierwagen, R. J. Kaplar and H. Umezawa, *J. Mater. Res.*, 2021, **36**, 4601-4615.
- <sup>6</sup> E. Berdermann and M. Ciobanu, in *CVD Diamond for Electronic Devices and Sensors*, ed. R. S. Sussmann, Wiley, New Jersey, 2009, ch. 10, pp. 227-255.
- <sup>7</sup> L. Tien and C. Ho, in *Gallium Oxide: Technology, Devices and Applications*, ed. S. Pearton, F. Ren and M. Mastro, Elsevier, Amsterdam, 2019, ch. 4, pp. 67-90.
- <sup>8</sup> C. E. Troupe, I. C. Drummond, C. Graham, J. Grice, P. John, J. I. B. Wilson, M. G. Jubber and N. A. Morrison, *Diamond Relat. Mater.*, 1998, **7**, 575-580.
- <sup>9</sup> A. W. Zia, S. A. Hussain, S. Rasul, D. Bae and S. Pitchaimuthu, *Journal of Energy Storage*, 2023, **72**, 108803.

- <sup>10</sup> W. Tillmann, *Int. J. Refract. Met. Hard Mater.*, 2000, **18**, 301-306.
- <sup>11</sup> V. Sittinger, S. Baron, M. Höfer, M. Armgardt and T. Harig, *Surf. Coat. Technol.*, 2023, **457**, 129287.
- <sup>12</sup> R. J. Hamers, J. E. Butler, T. Lasseter, B. M. Nicols, J. N. Russell Jr., K. Tse and W. Yang, *Diamond Relat. Mater.*, 2005, **14**, 661-668.
- <sup>13</sup> H. B. Salah, A. Hocini, M. N. Temmar and D. Khedrouche, *Chin. J. Phys. (Amsterdam, Neth.)*, 2019, **61**, 86-97.
- <sup>14</sup> J. Hornstra, *J. Phys. Chem. Solids*, 1957, **5**, 129-141.
- <sup>15</sup> Diamond – Molecule of the Month, <https://www.chm.bris.ac.uk/motm/diamond/diamond.htm>, (accessed April 2024).
- <sup>16</sup> *The Element Six CVD Diamond Handbook*, Element Six Technologies, 2021.
- <sup>17</sup> H. Gomez, M. N. Groves and M. R. Neupane, *Carbon Trends*, 2021, **3**, 100033.
- <sup>18</sup> U. Choi, H. Shin, T. Kwak, S. Kim and O. Nam, *Diamond Relat. Mater.*, 2022, **121**, 108770.
- <sup>19</sup> K. Kobashi, K. Nishimura, Y. Kawate and T. Horiuchi, *Phys. Rev. B*, 1988, **38**, 4067-4095.
- <sup>20</sup> A. Tallaire, J. Achard, A. Boussadi, O. Brinza, A. Gicquel, I. N. Kupriyanov, Y. N. Palyanov, G. Sakr and J. Barjon, *Diamond Relat. Mater.*, 2014, **41**, 34-40.
- <sup>21</sup> H. Kato, J. Barjon, N. Habka, T. Matsumoto, D. Takeuchi, H. Okushi and S. Yamasako, *Diamond Relat. Mater.*, 2011, **20**, 1016-1019.
- <sup>22</sup> D. Jain, J. Nuwad, N. Manoj and V. Sudarsan, in *Materials Under Extreme Conditions: Recent Trends and Future Prospects*, ed. A. K. Tyagi and S. Banerjee, Elsevier, Amsterdam, 2017, ch. 19, pp. 683-715.
- <sup>23</sup> M. Chandran, in *Carbon-Based Nanofillers and Their Rubber Nanocomposites: Carbon Nano-Objects*, ed. S. Yaragalla, R. Mishra, S. Thomas, N. Kalarikkal and H. J. Maria, Elsevier, Amsterdam, 2019, ch. 6, pp. 183-224.
- <sup>24</sup> S. S. Dossa, I. Ponomarev, B. N. Feigelson, M. Hainke, C. Kranert, J. Friedrich and J. J. Derby, *J. Cryst. Growth*, 2023, **609**, 127150.
- <sup>25</sup> D. Li, Q. Wang, X. Lv, L. Li and G. Zou, *J. Alloys. Compd.*, 2023, **960**, 170890.
- <sup>26</sup> S. Kim, Y. Kawamata, R. Takaya, K. Koyama and M. Kasu, *Appl. Phys. Lett.*, 2020, **117**, 202102.
- <sup>27</sup> X. Zhu, J. Liu, S. Shao, J. Tu, Y. Huang, T. Bi, L. Chen, J. Wei, H. Kawarada and C. Li, *Diamond Relat. Mater.*, 2021, **120**, 108640.
- <sup>28</sup> P. W. May, *Endeavour*, 1995, **19**, 101-106.
- <sup>29</sup> R. Haubner, *ChemTexts*, 2021, **7**, 10.
- <sup>30</sup> J. A. Smith, K. N. Rosser, H. Yaxgi, M. I. Wallace, P. W. May and M. N. R. Ashfold, *Diamond Relat. Mater.*, 2001, **10**, 370-375.
- <sup>31</sup> P. Hartmann, R. Haubner and B. Lux, *Diamond Relat. Mater.*, 1996, **5**, 850-856.
- <sup>32</sup> M. Bruno, L. Pastero, A. Cotellucci and D. Aquilano, *CrystEngComm*, 2022, **24**, 4165-4173.

- <sup>33</sup> P. W. May, in *Carbon Based Nanomaterials*, ed. N. Ali, A. Öchsner and W. Ahmed, Trans Tech, Switzerland, 2010, vol. 65-66, ch. 6, pp. 145-176.
- <sup>34</sup> J. Purushothaman, P. R. Sajanlal, M. Ponnaivaikko and T. Pradeep, *Diamond Relat. Mater.*, 2011, **20**, 1050-1055.
- <sup>35</sup> A. Zhou, H. Zhang, Q. Li and L. Xiao, in *Encyclopedia of Spectroscopy and Spectrometry*, ed. J. C. Lindon, G. E. Tranter and D. W. Koppenaal, Elsevier, Amsterdam, 3rd edn, 2017, pp. 18-25.
- <sup>36</sup> R. P. Van Duyne and C. L. Haynes, in *Encyclopedia of Physical Science and Technology*, ed. R. A. Meyers, Elsevier, Amsterdam, 3rd edn., 2003, pp. 845-866.
- <sup>37</sup> J. Filik, *Spectrosc. Eur.*, 2005, **17**, 10-17.
- <sup>38</sup> C. J. Chen, in *Introduction to Scanning Tunneling Microscopy*, Oxford University Press, Oxford, 2nd edn, 2016, ch. 1, pp. 23-39.
- <sup>39</sup> Scanning Tunneling Microscope (STM), <https://afm.oxinst.com/modes/scanning-tunneling-microscopy-stm>, (accessed April 2024).
- <sup>40</sup> D. Kabanov, S. Klimovic, V. Rotrekl, M. Pesl and J. Pribyl, *Micron*, 2022, **155**, 103199.
- <sup>41</sup> N. Fleck, H. Amli, V. Dhanak and W. Ahmed, in *Emerging Nanotechnologies for Renewable Energy: Micro and Nano Technologies*, ed. W. Ahmed, M. Booth and E. Nourafkan, Elsevier, Amsterdam, 2021, ch. 11, pp. 259-285.
- <sup>42</sup> M. Gonon, in *Encyclopedia of Materials: Technical Ceramics and Glasses*, ed. M. Pomeroy, Elsevier, Amsterdam, 2021, vol. 1, pp. 560-577.
- <sup>43</sup> S. Nasrazadani and S. Hassani, in *Handbook of Materials Failure Analysis With Case Studies from the Oil and Gas Industry*, ed. A. S. H. Makhlof and M. Aliofkhaezai, Elsevier, Amsterdam, 2016, ch. 2, pp. 39-54.
- <sup>44</sup> Diamond films on Planar (Flat) Substrates, <https://www.chm.bris.ac.uk/pt/diamond/semflat.htm>, (accessed April 2024).
- <sup>45</sup> F. Adams and C. Barbante, *Compr. Anal. Chem.*, 2015, **69**, 67-124.
- <sup>46</sup> Q. Liang, C. Y. Chin, J. Lai, C. Yan, Y. Meng, H. Mao and R. J. Hemley, *Appl. Phys. Lett.*, 2009, **94**, 024103.
- <sup>47</sup> K. W. Hemawan and R. J. Hemley, *J. Vac. Sci. Technol., A*, 2015, **33**, 061302.
- <sup>48</sup> A. N. Goyette, J. E. Lawler, L. W. Anderson, D. M. Gruen, T. G. McCauley, D. Zhou and A. R. Krauss, *Plasma Sources Sci. Technol.*, 1998, **7**, 149-153.
- <sup>49</sup> K. K. Hirakuri, T. Kobayashi, E. Nakamura, N. Mutsukura, G. Friedbacher and Y. Machi, *Vacuum*, 2001, **63**, 449-454.
- <sup>50</sup> B. Song, H. Kim, K. Kim, J. Yang and N. Hwang, *Materials (Basel)*, 2021, **14**, 426.
- <sup>51</sup> D. Li, D. Zuo, W. Lu, R. Chen, B. Xiang and M. Wang, *Solid State Ionics*, 2008, **179**, 1263-1267.
- <sup>52</sup> A. Boudina, E. Fitzer and G. Wahl, *Diamond Relat. Mater.*, 1992, **1**, 248-254.
- <sup>53</sup> X. Yan, J. Wei, J. Guo, C. Hua, J. Liu, L. Chen, L. Hei and C. Li, *Diamond Relat. Mater.*, 2017, **73**, 39-46.

<sup>54</sup> *Introduction to Spectroscopy*, Royal Society of Chemistry, 2009.

<sup>54</sup> R. C. Dante, D. G. Dante, P. Martín-Ramos, P. Chamorro-Posada, M. C. Valsania, *Fullerenes, Nanotubes Carbon Nanostruct.*, 2022, **30**, 667-674.

<sup>55</sup> S. Yoshioka, in *Pattern Formations and Oscillatory Phenomena*, ed. S. Kinoshita, Elsevier, Amsterdam, 2013, ch. 6, pp. 199-251.

## 9. Appendix

### 9.1. Raman Spectroscopy of the Mo Substrate from the 1<sup>st</sup> CVD Reaction

For the first CVD reaction (with Mo substrate), six Raman spectroscopy measurements were conducted to investigate the composition of the surface layer on the molybdenum substrate (Fig. A1.2 to Fig. A1.7). Each Raman spectroscopy data corresponds to one of the regions in Fig. A1.1.

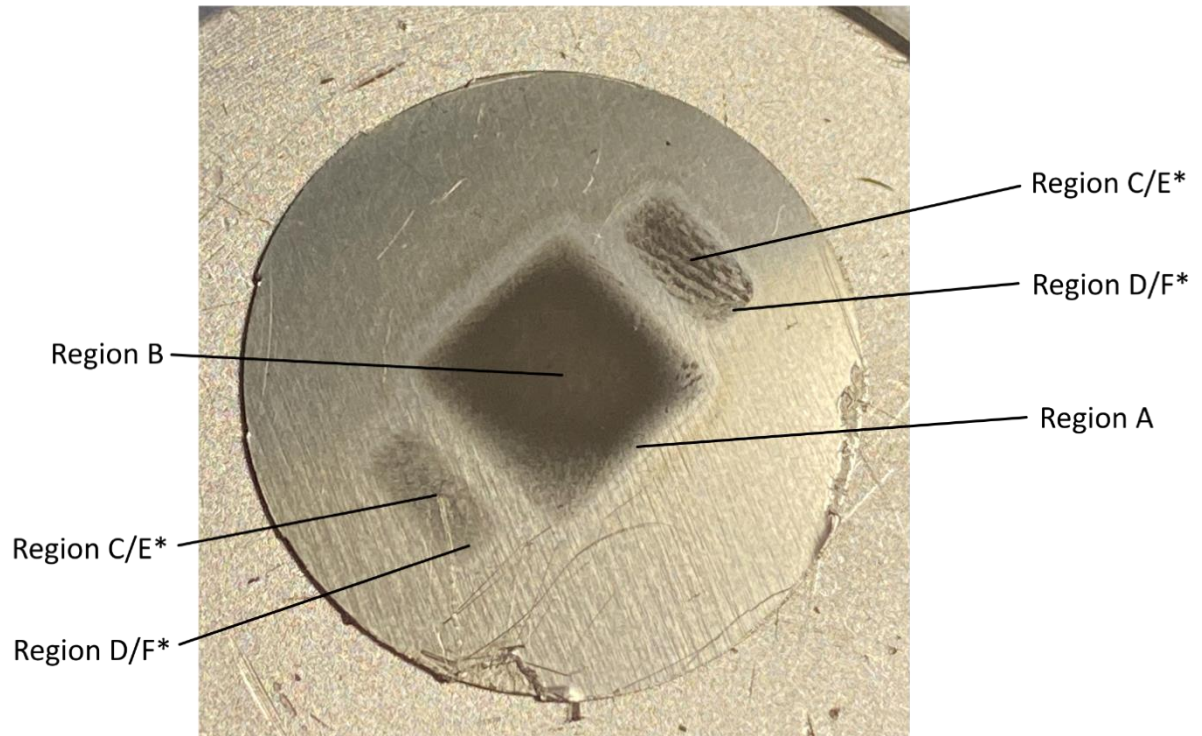
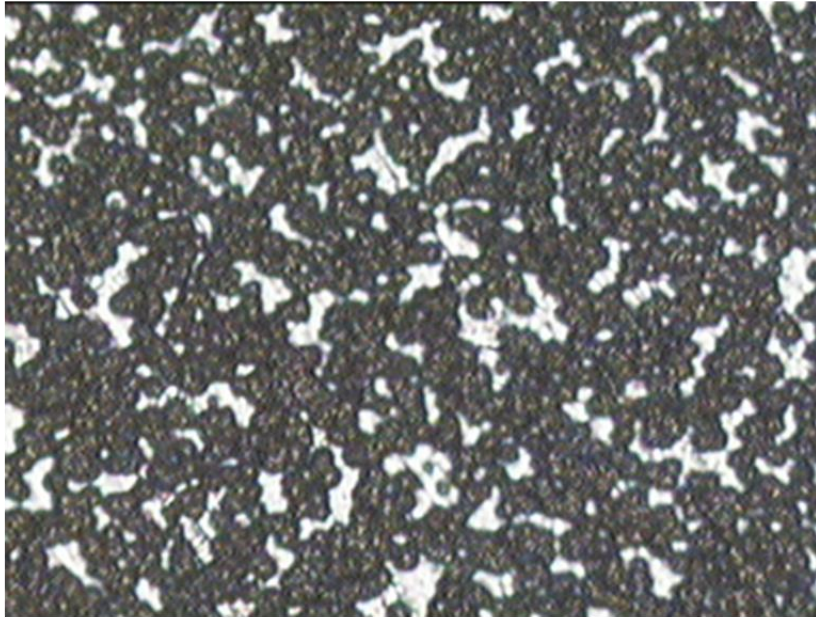


Figure A1.1: A photo of the Mo substrate after the CVD reaction. The same figure was displayed in Section 6.1 as Figure 19. (\*It was unclear which rectangular mark corresponded to Region C or E, and the same for the periphery regions D and F.)

a)



b)

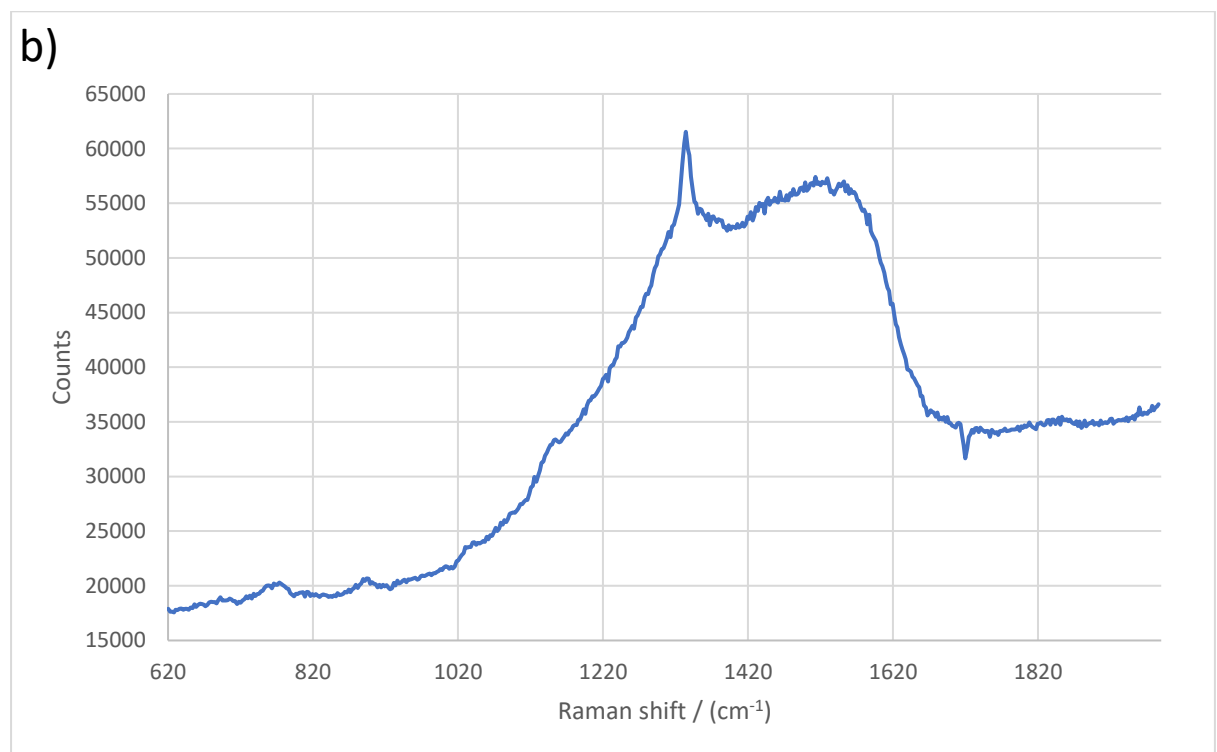


Figure A1.2: (a) Screenshot of the live video of Region A under Raman microscope. (b) Raman spectrum of Region A (Raman shift: 1334.33 cm<sup>-1</sup>).

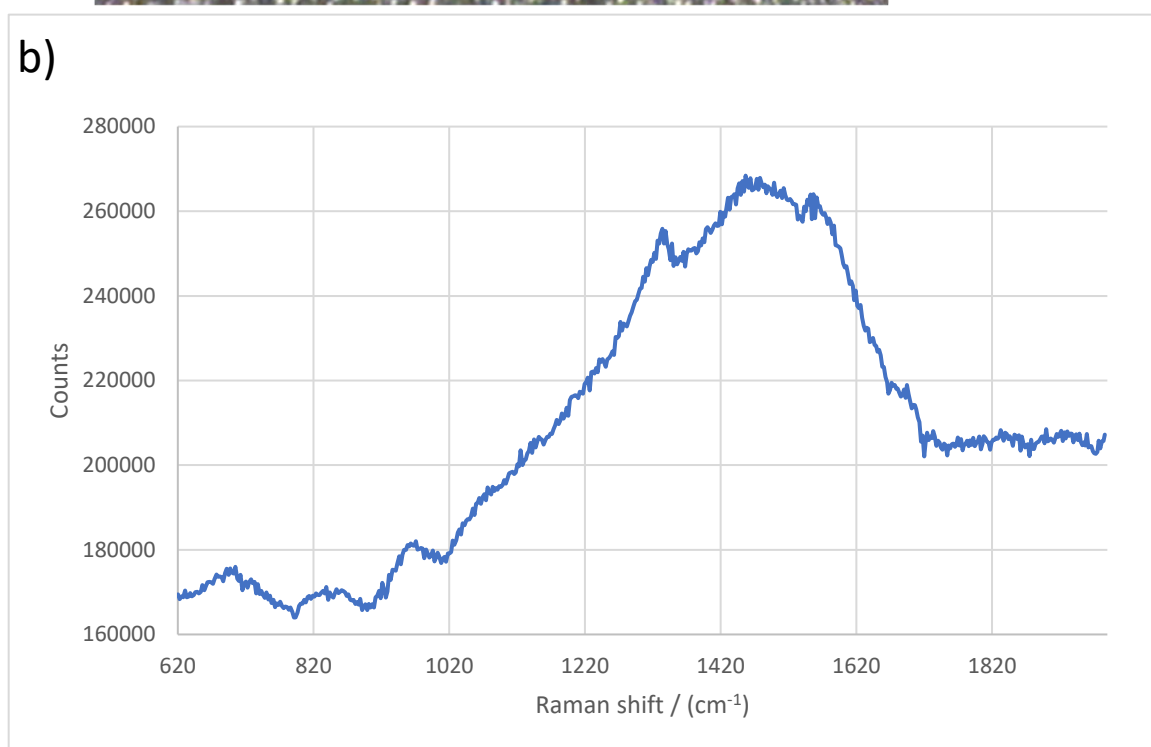


Figure A1.3: (a) Screenshot of the live video of Region B under Raman microscope. (b) Raman spectrum of Region B (Raman shift: 1332.44 cm<sup>-1</sup>).

a)



b)

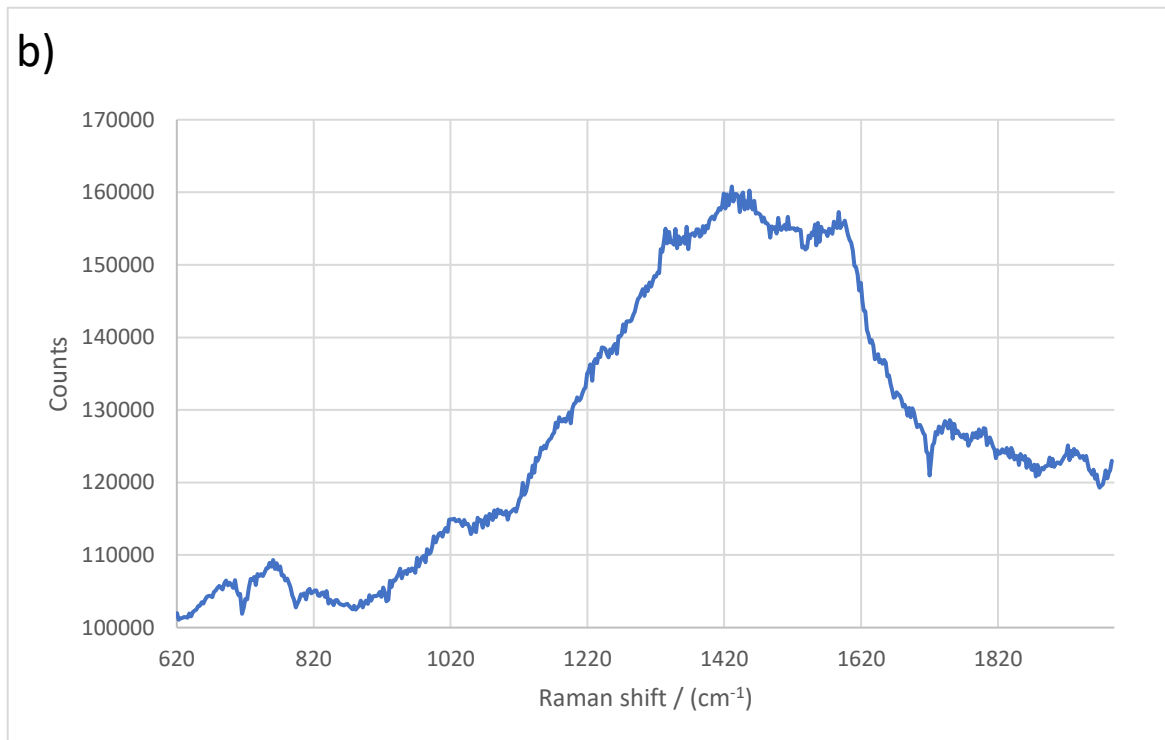


Figure A1.4: (a) Screenshot of the live video of Region C under Raman microscope. (b) Raman spectrum of Region C (Raman shift: 1338.71 cm<sup>-1</sup>).

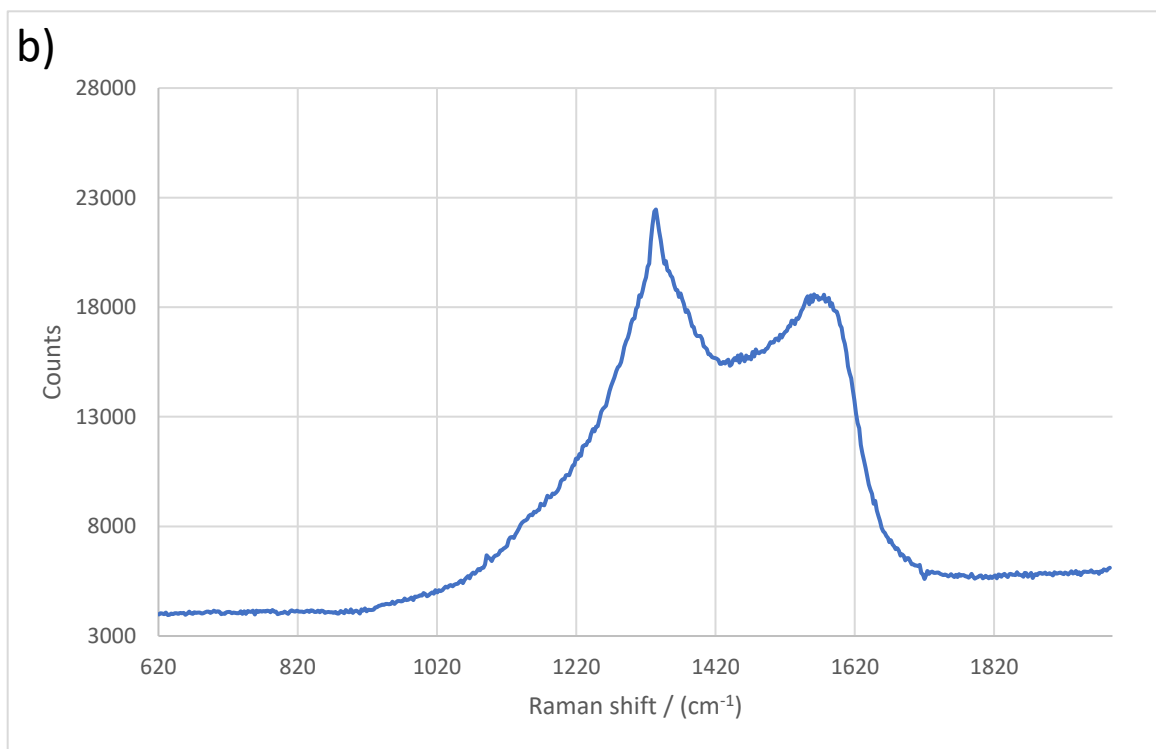
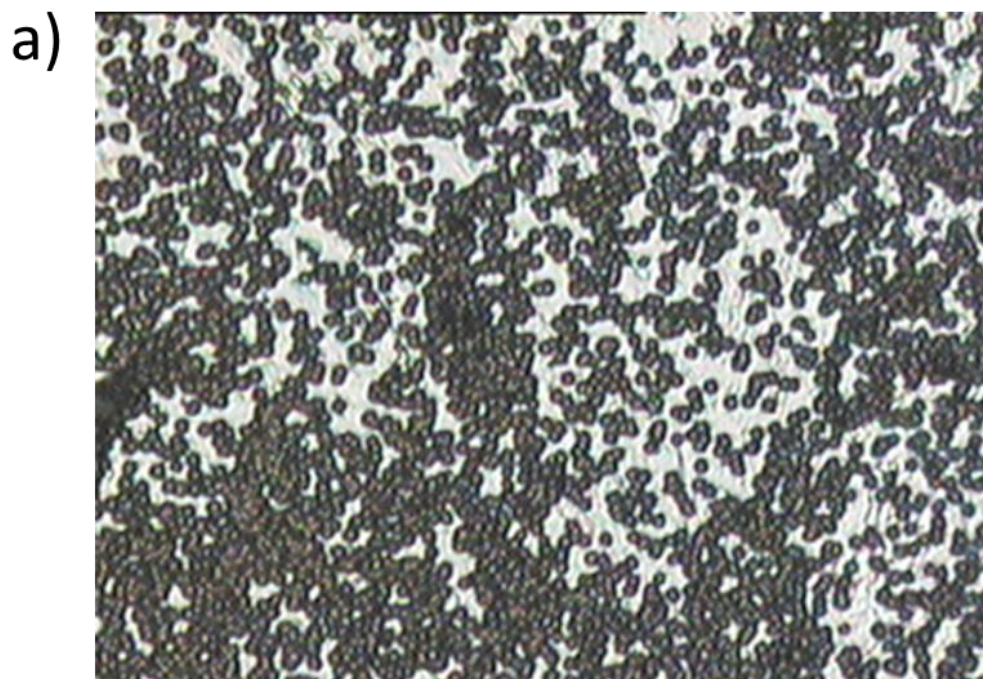


Figure A1.5: (a) Screenshot of the live video of Region C under Raman microscope. (b) Raman spectrum of Region C (Raman shift: 1332.44 cm<sup>-1</sup>).

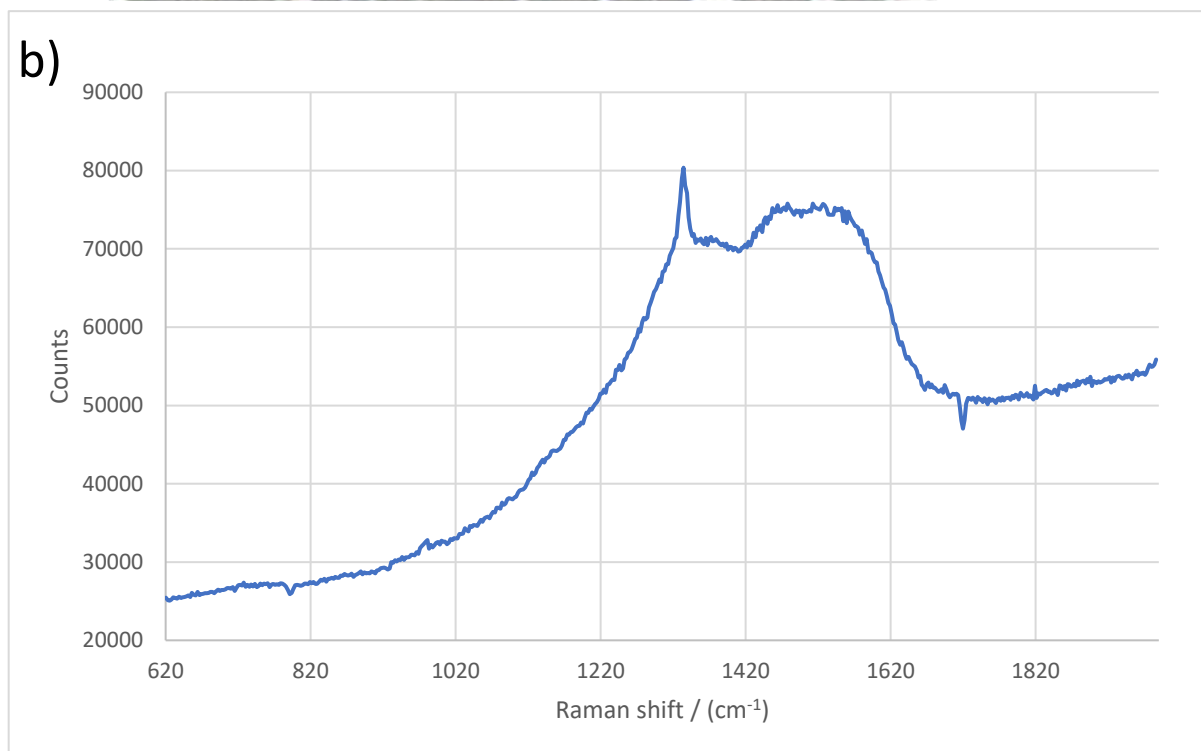
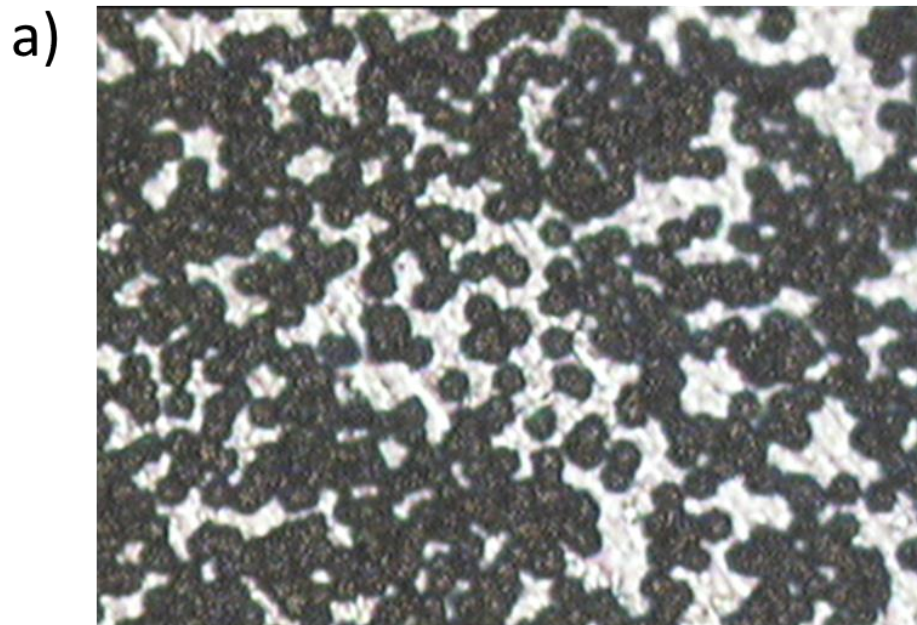
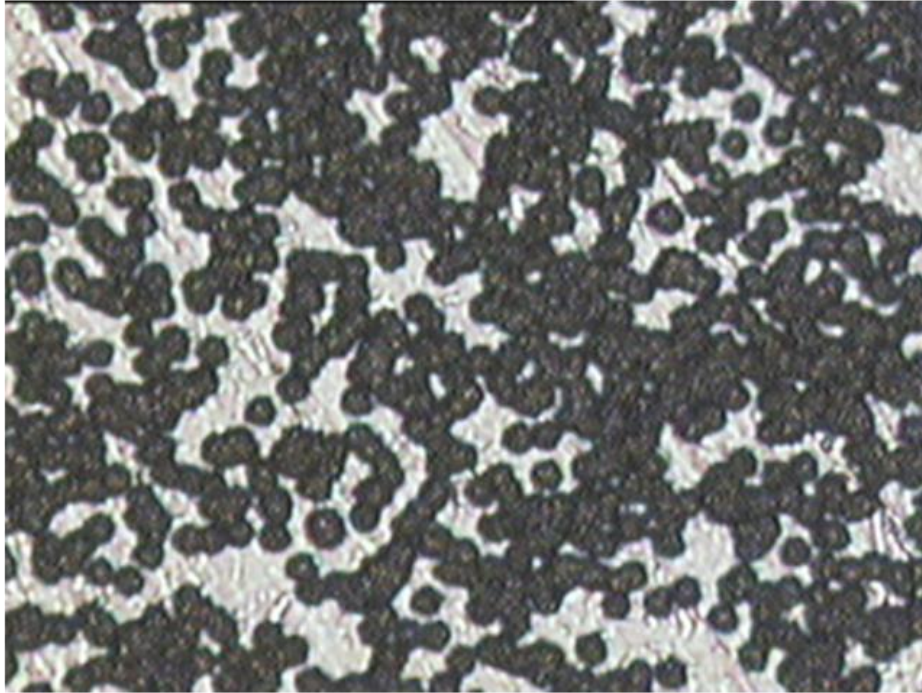


Figure A1.6: (a) Screenshot of the live video of Region C under Raman microscope. (b) Raman spectrum of Region C (Raman shift: 1334.52 cm<sup>-1</sup>).

a)



b)

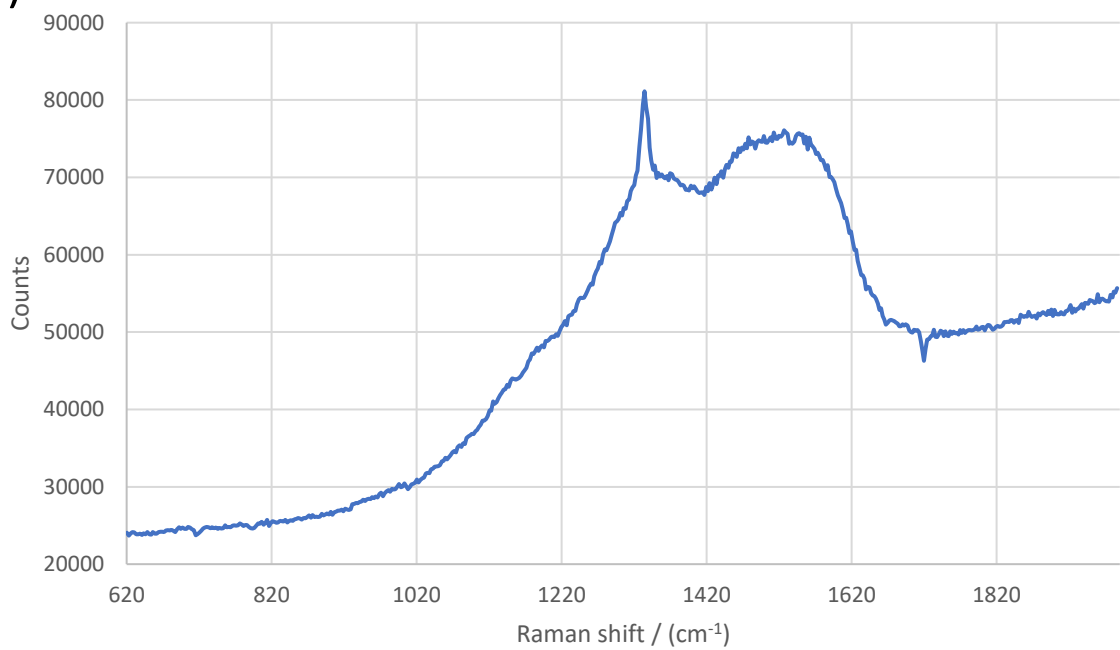


Figure A1.7: (a) Screenshot of the live video of Region C under Raman microscope. (b) Raman spectrum of Region C (Raman shift:  $1334.78 \text{ cm}^{-1}$ ).

## 9.2. Raman Spectroscopy of the Ir/sapphire Substrate on Mo disc from the 2<sup>nd</sup> CVD Reaction

For the second CVD reaction (with Ir/sapphire), two Raman spectroscopy measurements were made on the Ir/sapphire chips (Fig. A2.2 and Fig. A2.3). Three Raman spectroscopy measurements were conducted on the molybdenum substrate (Fig. A2.4 to Fig. A2.6), which was holding the Ir/sapphire chips on the anode of the reactor. Each Raman spectroscopy data corresponds to one of the regions in Fig. A2.1.

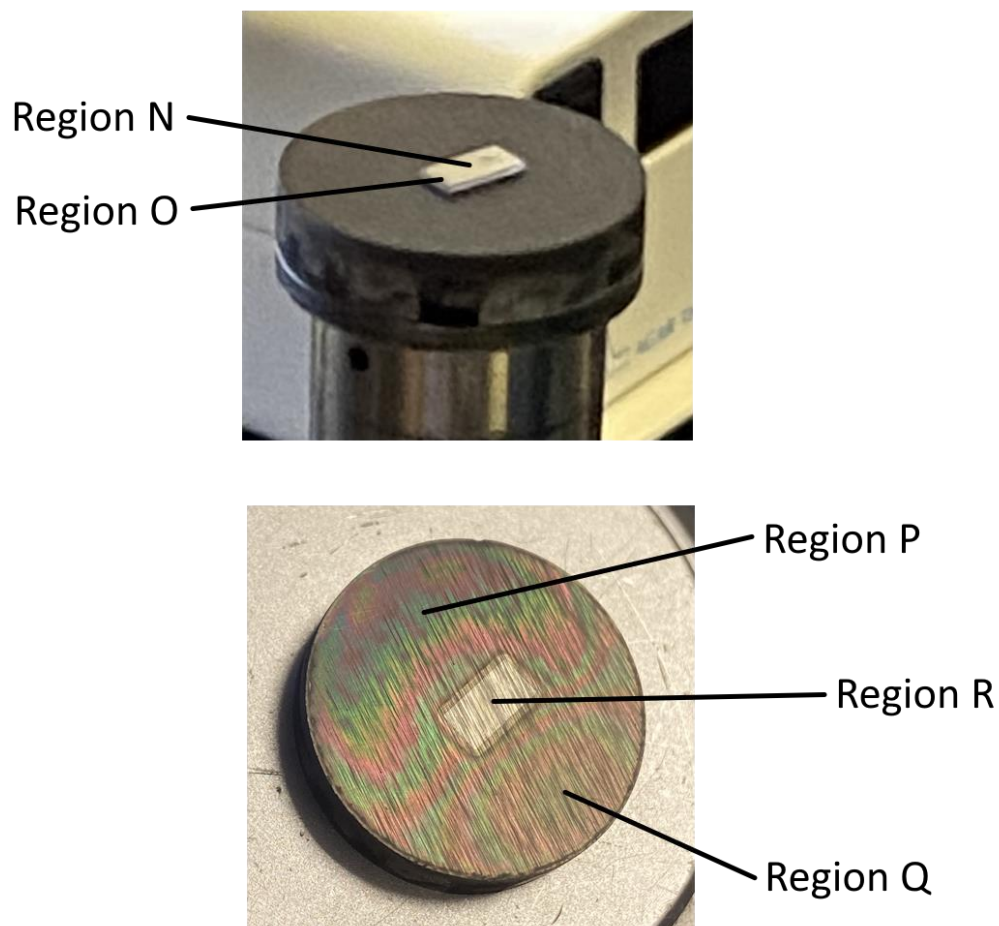
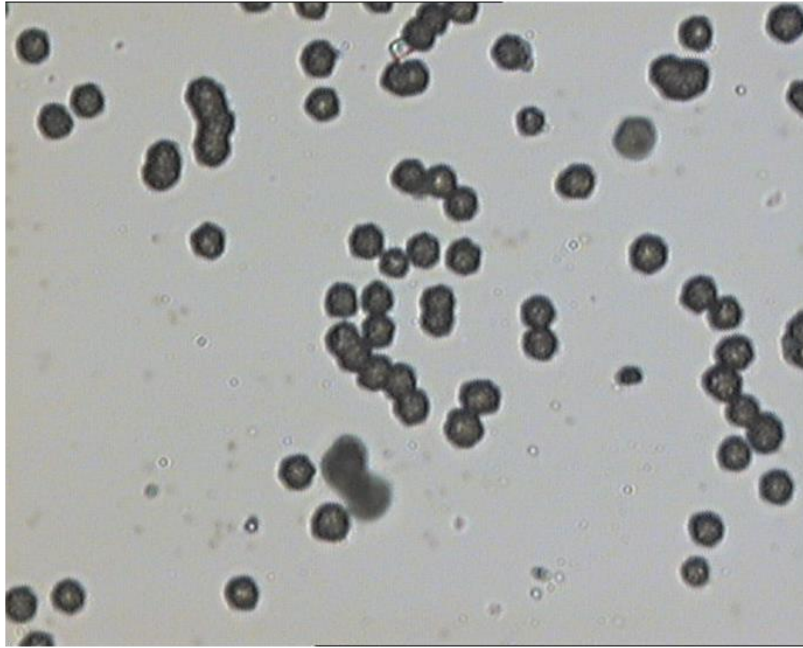


Figure A2.1: Labeled photos of the iridium/sapphire chip (top) and the molybdenum supporting disc (bottom). Region N and O correspond to the centre and the periphery of the Ir/sapphire substrate. Region P corresponds to the area on the Mo disc where the surface had a strong iridescent effect. Region Q corresponds to the area on the opposite side of Region Q. Region R corresponds to the centre of the disc, where the Ir/sapphire substrate was placed during the reaction.

a)



b)

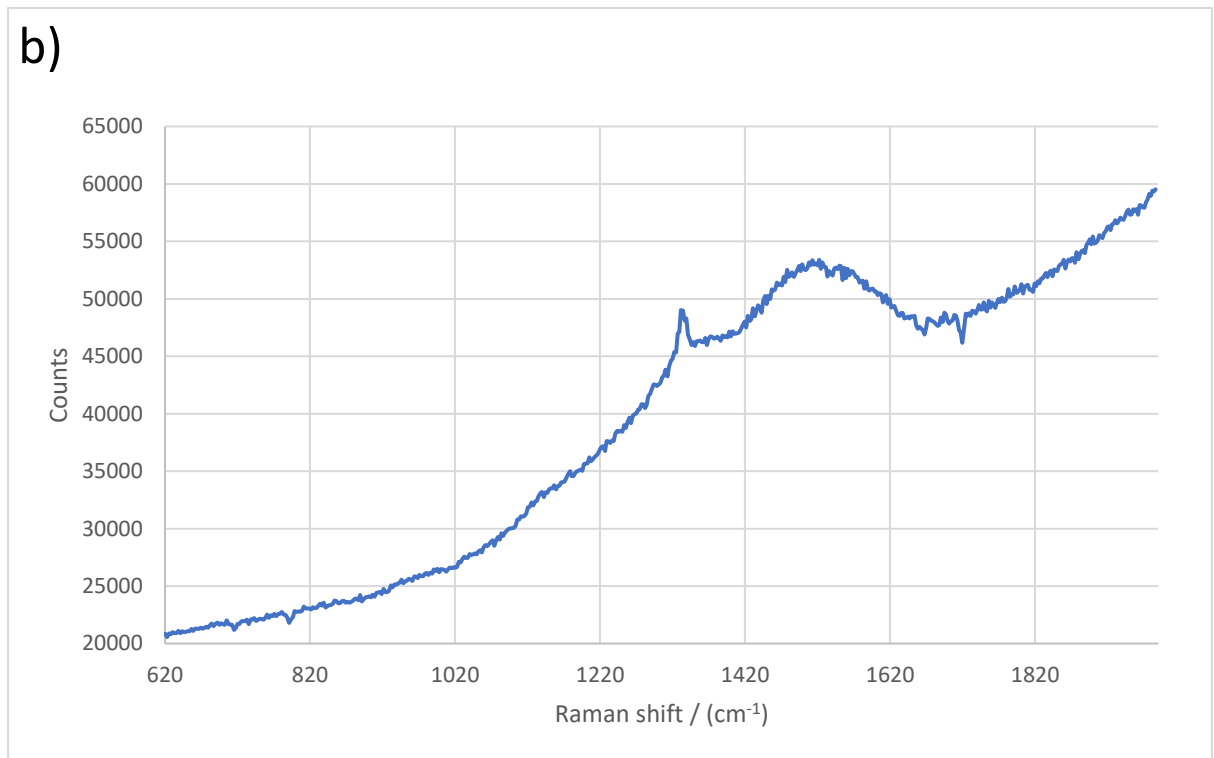


Figure A2.2: (a) Screenshot of the live video of Region N under Raman microscope. (b) Raman spectrum of Region N (Raman shift: 1333.61 cm<sup>-1</sup>).

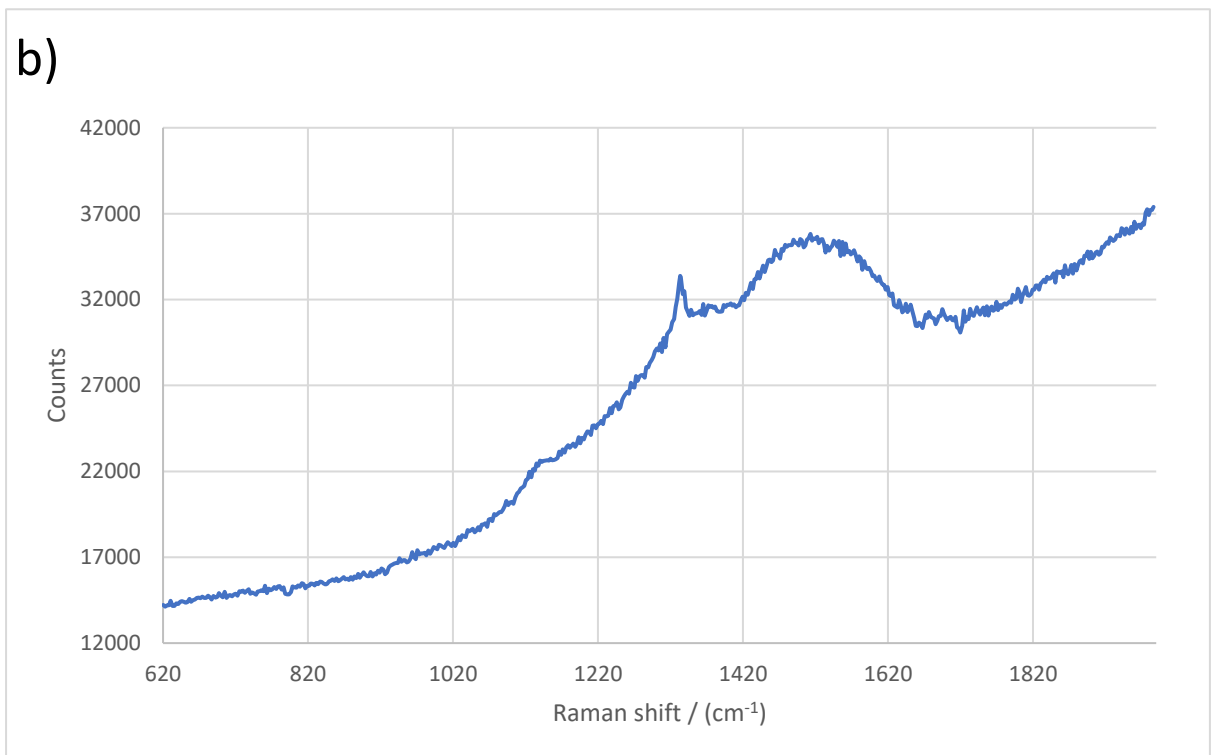
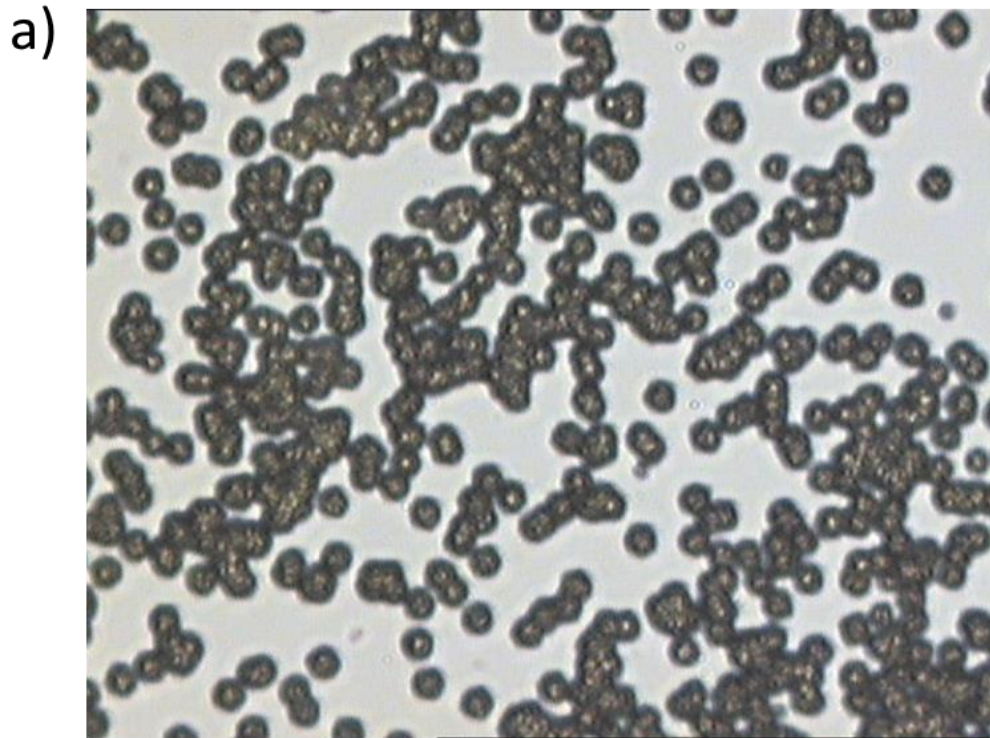
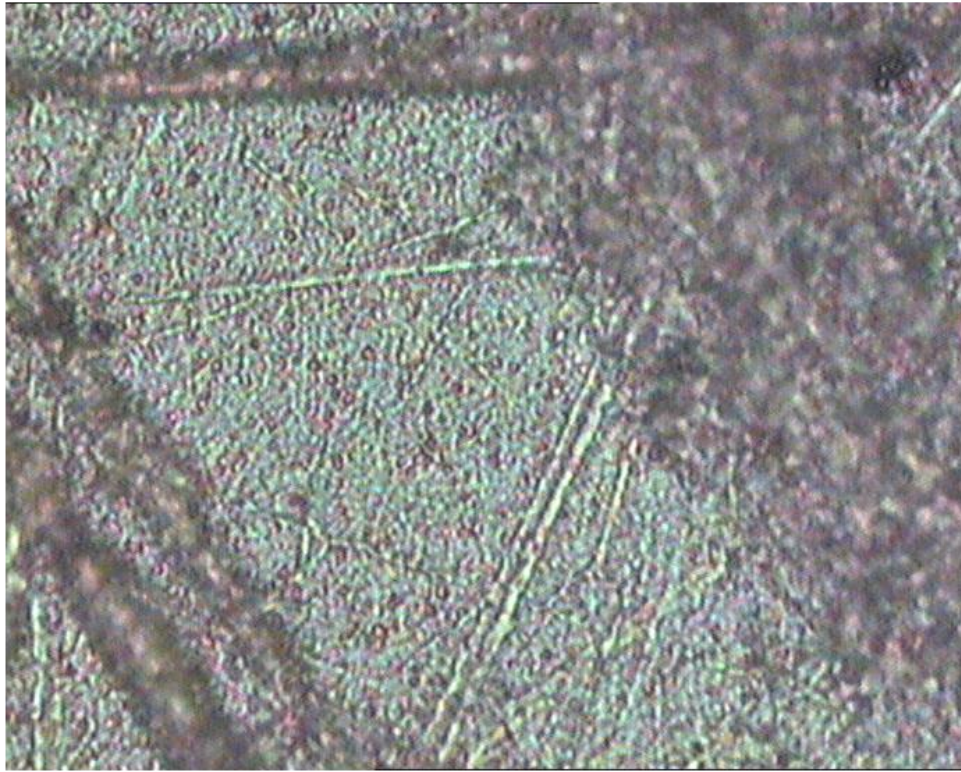


Figure A2.3: (a) Screenshot of the live video of Region O under Raman microscope. (b) Raman spectrum of Region O (Raman shift:  $1333.22 \text{ cm}^{-1}$ ).

a)



b)

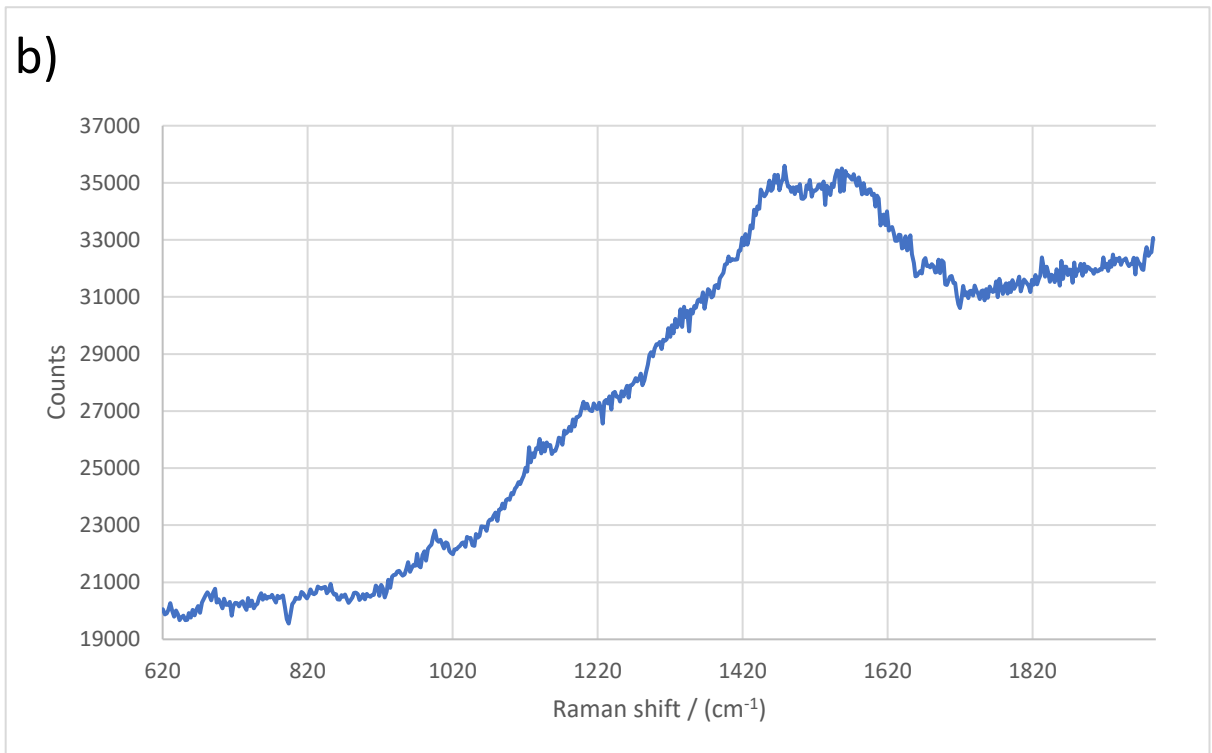


Figure A2.4: (a) Screenshot of the live video of Region P under Raman microscope. (b) Raman spectrum of Region P. There is no significant peak with the Raman shift at the diamond region.

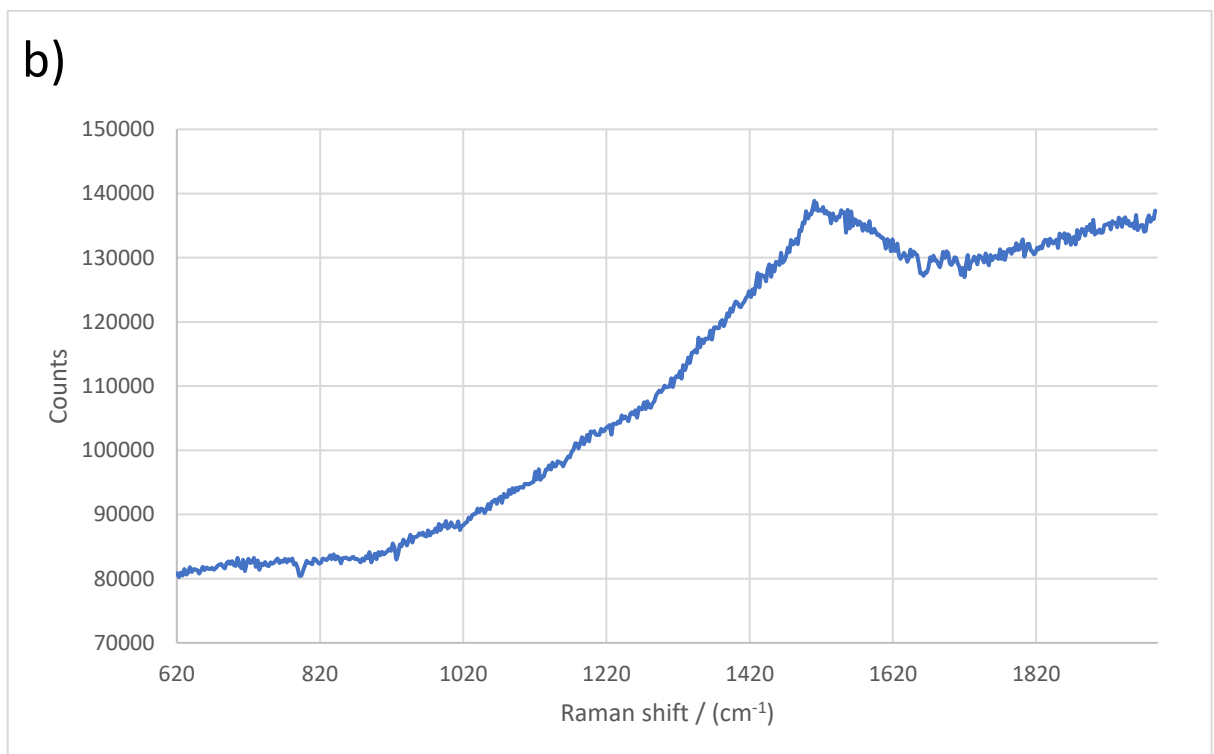
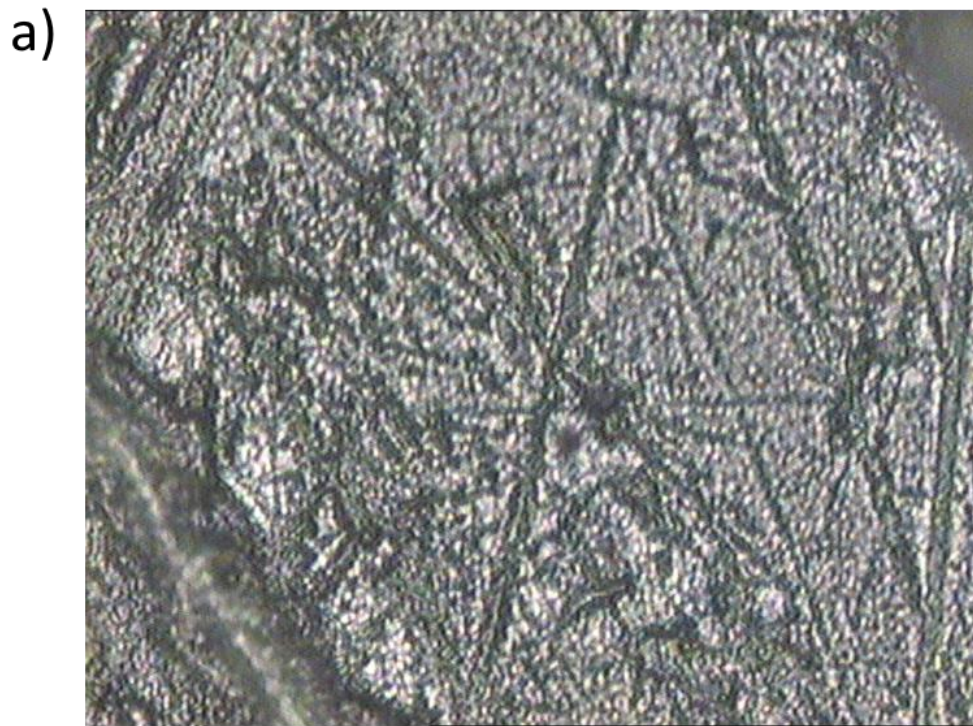


Figure A2.5: (a) Screenshot of the live video of Region Q under Raman microscope. (b) Raman spectrum of Region Q. There is no significant peak with the Raman shift at the diamond region.

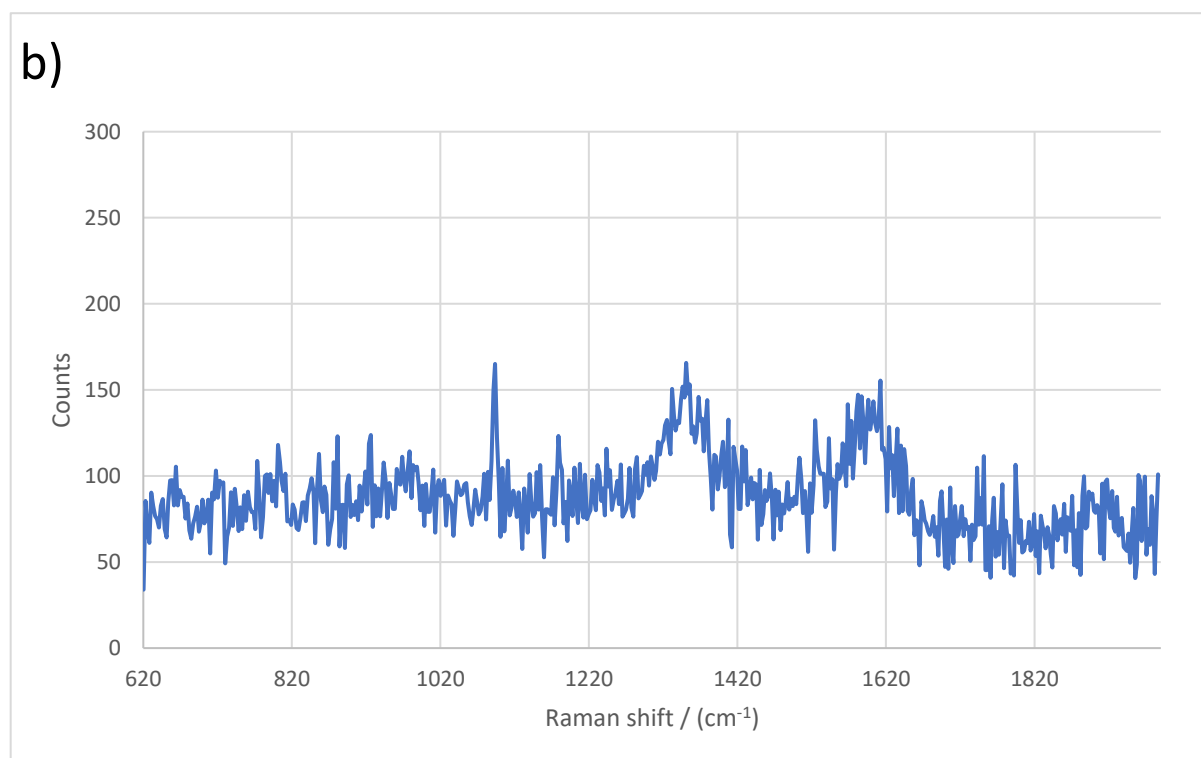
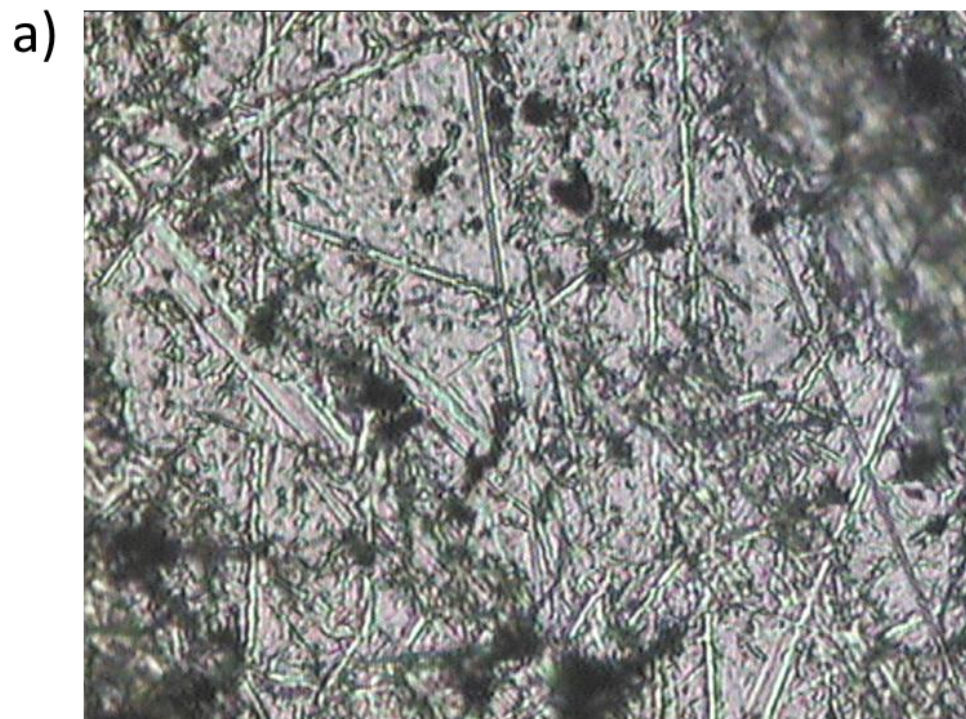


Figure A2.6: (a) Screenshot of the live video of Region R under Raman microscope. (b) Raman spectrum of Region R. The spectrum has a similar shape to the Raman spectrum of a molybdenum substrate with no surface deposition (refer to Fig. 27 in Section 6.2).

### 9.3. Optical Emission Spectroscopy of the 2<sup>nd</sup> CVD Reaction

Real-time optical emission spectroscopy was conducted during the second CVD reaction with Ir/sapphire substrate. Fig. A3.1 shows a snapshot of the OES spectrum during the reaction, and Fig. A3.2 shows the same spectrum but zoomed in, showing only the visible light region.

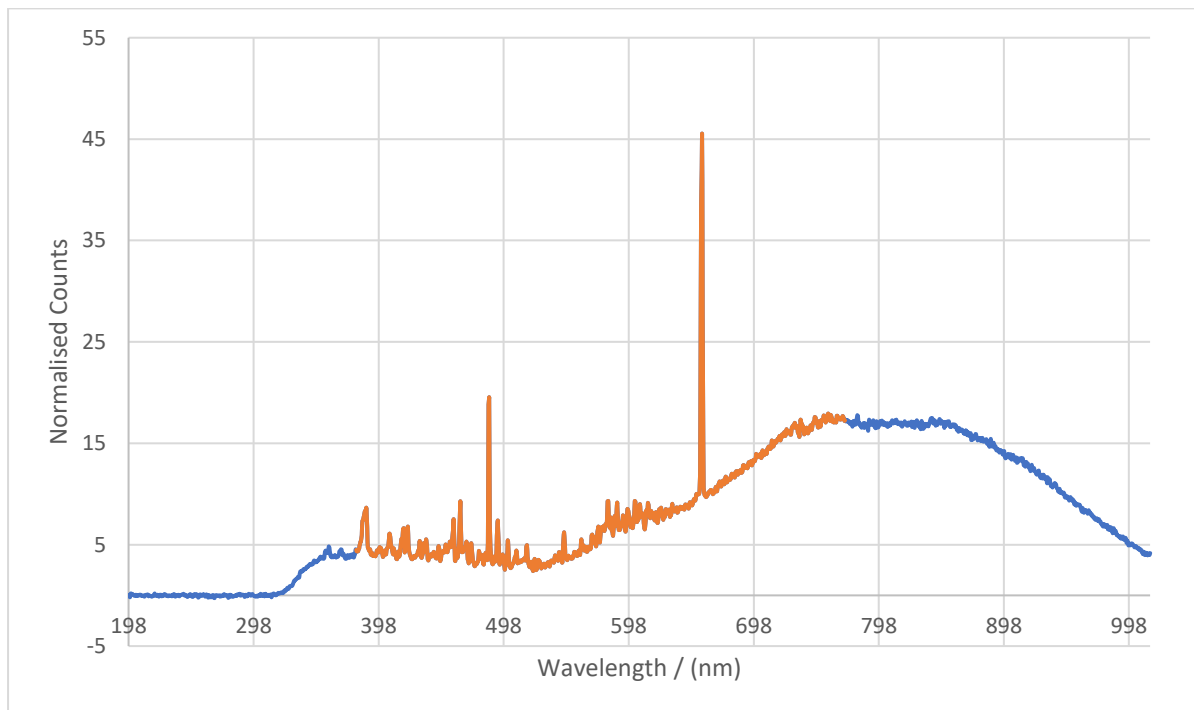


Figure A3.1: Optical emission spectrum of the plasma during the second CVD reaction with Ir/sapphire substrate. The orange region corresponds to the visible region (380 nm to 770 nm).

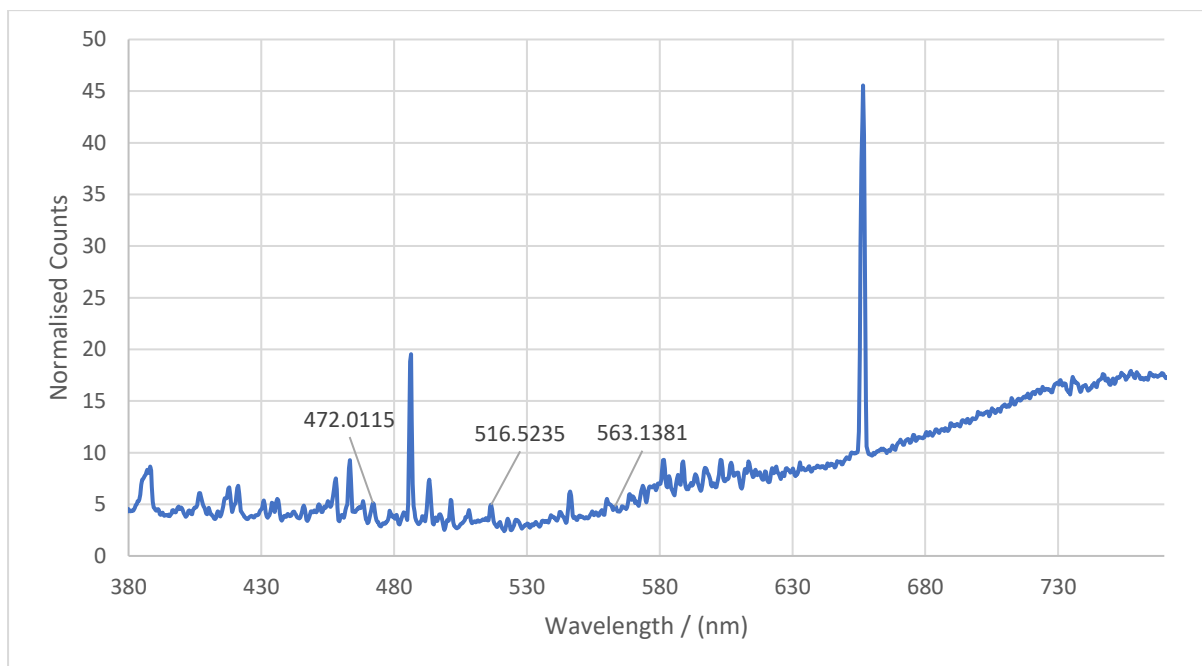


Figure A3.3: A zoomed-in optical emission spectrum of Fig. A3.2, showing only the visible light region (from 380 nm to 770 nm).<sup>54</sup> The three labelled peaks correspond to C<sub>2</sub> emission peaks (471.55, 516.52 and 563.25 nm).<sup>47</sup>

9.4. Lab Clearance Form

Laboratory Clearance: Check List

<b>Name of Researcher</b> <i>Chen Hui Lui</i>	<b>Laboratories/Work Areas</b> <i>Diamond Laboratory</i>
<p><b>Chemicals</b></p> <p>Search out and evaluate all chemicals and label all containers.</p> <p>Transfer responsibility for material to:              signed <i>[Signature]</i></p> <p>Prepare chemical waste for disposal.</p> <p>Clean glassware, refrigerators, ovens etc.</p> <p>Clean working area.</p> <p>Sign out.</p> <p><b>Radioactive Material</b></p> <p>Label and secure material. Check for Stock Cards.</p> <p>Dispose of waste. Update Stock Cards.</p> <p>Transfer responsibility for material to:              signed.....</p> <p>Update Stock Cards.</p> <p>Departing group leaving material inform DRPS and Safety Office in writing.              Permission obtained in writing (copy attached).</p> <p>Clean and decontaminate the working area.              Approval of University RPS obtained (copy attached).</p> <p>Sign out.</p>	<p><b>Micro-organisms and Cultures</b></p> <p>Label and secure material.</p> <p>Autoclave waste.</p> <p>Clean glassware, incubators, ovens, refrigerators.</p> <p>Transfer responsibility for material to:              signed.....</p> <p>Decontaminate and clean the working area.</p> <p>Sign out.</p> <p><b>Mixed Hazard Material</b></p> <p>Complete the appropriate clearing and decontamination procedures outlined above.</p> <p><b>Equipment</b></p> <p>Unwanted equipment decontaminated and cleared to waste.</p> <p>Equipment to be left transferred to:              signed.....</p> <p>Custom equipment instructions and risk assessment.</p> <p>Gas Cylinders to Store.</p> <p>Clean the working area.</p> <p>Sign out.</p>

**All clearing procedures have been completed.**

Signature Researcher ..... *[Signature]* ..... Date *19/3/2024*

Signature Research Supervisor/Head of Section..... *[Signature]* ..... Date *19/3/2024* (Dr James Smith)

**A copy of this form, completed and signed should be returned with your thesis.**